INTERNATIONAL JOURNAL FOR NUMERICAL METHODS IN FLUIDS
Int. J. Numer. Meth. Fluids 2007; **54**:119–154
Published online 28 November 2006 in Wiley InterScience (www.interscience.wiley.com). DOI: 10.1002/fld.1387

On the construction of manufactured solutions for one and two-equation eddy-viscosity models

L. Eça[1,*,†,‡], M. Hoekstra[2,§], A. Hay[3,¶] and D. Pelletier[3,‖]

[1]*Instituto Superior Técnico, Department of Mechanical Engineering, Av. Rovisco Pais, 1049-001 Lisbon, Portugal*
[2]*Maritime Research Institute Netherlands, P.O. Box 28 6700 AA, Wageningen, The Netherlands*
[3]*Ecole Polytechnique de Montréal, Department of Mechanical Engineering, Montréal, Canada C.P. 6079*

SUMMARY

This paper presents manufactured solutions (MSs) for some well-known eddy-viscosity turbulence models, viz. the Spalart & Allmaras one-equation model and the TNT and BSL versions of the two-equation k–ω model. The manufactured flow solutions apply to two-dimensional, steady, wall-bounded, incompressible, turbulent flows. The two velocity components and the pressure are identical for all MSs, but various alternatives are considered for specifying the eddy-viscosity and other turbulence quantities in the turbulence models.

The results obtained for the proposed MSs with a second-order accurate numerical method show that the MSs for turbulence quantities must be constructed carefully to avoid instabilities in the numerical solutions. This behaviour is model dependent: the performance of the Spalart & Allmaras and k–ω models is significantly affected by the type of MS. In one of the MSs tested, even the two versions of the k–ω model exhibit significant differences in the convergence properties. Copyright © 2006 John Wiley & Sons, Ltd.

Received 5 July 2006; Revised 29 August 2006; Accepted 6 September 2006

KEY WORDS: manufactured solutions; code verification; eddy-viscosity; turbulence models

1. INTRODUCTION

The first step in checking the reliability of a computational fluid dynamics tool is code verification. In this context, the method of manufactured solution (MMS), [1–7], is a very useful technique, because it provides a general procedure for working with analytical solutions.

*Correspondence to: L. Eça, Instituto Superior Técnico, Department of Mechanical Engineering, Av. Rovisco Pais, 1049-001 Lisbon, Portugal.
†E-mail: eca@marine.ist.utl.pt
‡Assistant Professor.
§Senior Research Scientist.
¶Post-doctoral Fellow.
‖Professor, Canada Research Chair.

Recently, a manufactured solution (MS) has been proposed for code and calculation verification of two-dimensional, steady, wall-bounded, incompressible, turbulent flows [8]. This MS is defined in a square domain where the bottom boundary is an impermeable, no-slip wall. The MS specifies the two velocity components, the pressure, the eddy-viscosity and any additional turbulence quantity required by the transport equations pertinent to six different turbulence models:

- Spalart & Allmaras one-equation model, [9].
- Menter's one-equation model, [10].
- Standard k–ε two-equation model, [11].
- Chien's low-Reynolds k–ε two-equation model, [12].
- The turbulent/non-turbulent (TNT) k–ω two-equation model, [13].
- Menter's baseline (BSL) k–ω two-equation model, [14].

Initially, the part of the MS related to the turbulence model included manufactured functions for the eddy-viscosity and the turbulence kinetic energy only; other turbulence quantities required were derived from them. It has turned out, however, (see [8]), that in the context of a MS the specification of the eddy-viscosity in the one-equation models is troublesome due to the behaviour of the damping functions used in the models. Therefore, for the Spalart & Allmaras and Menter one-equation models the MS specifies the dependent variable of the model (i.e. the damped eddy-viscosity) instead of the eddy-viscosity itself.

Although the purpose of the MS is not to evaluate or compare turbulence models, one might feel tempted to compare the numerical performance obtained with different turbulence models. However, such comparisons are often unfair. For example, in the MS proposed in [8], the MSs fields for k, ε and ω are simpler than the manufactured eddy-viscosity, ν_t. Thus, one-equation models are 'penalized' in such comparisons. However, if a given model leads to an unexpected poor performance of the flow solver for a given MS, it is important to find the reasons for such behaviour.

Results obtained with the finite-difference version of PARNASSOS, [15], for the calculation of the proposed MS have been presented in an earlier technical report, [16], Three types of exercises were performed:

1. Numerically solve the turbulence model transport equation(s) using the known manufactured velocity field.
2. Calculate the velocity and pressure field using the known manufactured eddy-viscosity.
3. Compute the complete flow field coupling flow and turbulence variables.

The first and third exercises were performed for the six turbulence models considered in [8].

The results presented in [16] show that it is relatively straightforward to attain the asymptotic range in the solution of the continuity and momentum equations with the manufactured eddy-viscosity field (exercise 2 of the list above). In exercise 3, however, the solution of the turbulence quantities transport equations appears to have a significant effect on the observed order of accuracy of the main flow quantities for the same grid density. We found that with the four two-equation models tested, the observed orders of accuracy are not as well behaved as those obtained with the manufactured ν_t, but they are still close to the theoretical order of the method. However, the results obtained with the one-equation turbulence models exhibit an irregular behaviour of the observed order of accuracy, p, which in the case of the Spalart & Allmaras model is clearly below the theoretical order of the method. With this turbulence model, results from exercise 1 (the calculation of the eddy-viscosity with the manufactured velocity field) revealed that the

DOI: 10.1002/fld

near-wall solution of the dependent variable, $\tilde{\nu}$, converges very slowly. Therefore, it is important to investigate the reasons for such behaviour and get some insight into the cause of the difficulties.

In this paper we present and compare alternative formulations for the manufactured turbulence quantities included in three of the six turbulence models considered in [8]: the one-equation model of Spalart & Allmaras and the TNT and BSL versions of the k–ω model.

For the one-equation model of Spalart & Allmaras, we define three MSs which differ in the behaviour of the turbulence quantity, $\tilde{\nu}$, in the near-wall region. In the original MS, [8], $\tilde{\nu}$ in the near-wall region varies with the fourth power of the distance to the bottom. The two alternative MSs presented in this paper depend on the second and first powers of the distance to the bottom.

The specified distributions of $\tilde{\nu}$ proposed for the Spalart & Allmaras model are equal to the distributions of eddy-viscosity, ν_t, specified for the two versions of the k–ω model. In the two-equation models, the second manufactured quantity is the turbulence kinetic energy, k. In two of the MSs tested, the manufactured k is similar to ν_t, but with a lower order dependency on the distance to the bottom than ν_t (i.e. $k \sim y^2$ when $\nu_t \sim y^4$ and $k \sim y$ when $\nu_t \sim y^2$). We have also tested three alternative MSs where k is obtained from Bradshaw's hypothesis of equilibrium turbulence. These five alternative MSs lead to different boundary conditions and different 'near-wall' behaviour for k and ω.

In both cases, one and two-equation models, only the original MS, [8], represents the expected physical behaviour of a near-wall turbulent flow. However, the behaviour of the turbulence quantities reproduced in the MSs may not be as local as one would expect in a real turbulent flow.

The paper is organized as follows: Section 2 presents the proposed MSs, which for the sake of completeness include also the main flow variables; the results of the numerical calculations of the MSs with a second-order method are presented and discussed in Section 3. The conclusions of this paper are summarized in Section 4. The source terms required to satisfy the turbulence quantities transport equations are presented in the Appendix. The minimum and maximum values of all the terms of the momentum equations and turbulence quantities transport equations, including the manufactured source terms, are also included in the Appendix.

2. MANUFACTURED SOLUTIONS

2.1. Computational domain

The computational domain is a square of side $0.5L$ with $0.5L \leqslant X \leqslant L$ and $0 \leqslant Y \leqslant 0.5L$ and the Reynolds number, Re, is 10^6

$$Re = \frac{U_1 L}{\nu} \tag{1}$$

where U_1 is the reference velocity, L the reference length and ν the kinematic viscosity. In non-dimensional variables, (x, y), the computational domain is given by $0.5 \leqslant x \leqslant 1$ and $0 \leqslant y \leqslant 0.5$, where x stands for the horizontal direction and y for the vertical direction.

2.2. Main flow variables

In the definition of the velocity components and pressure coefficient we will use the following non-dimensional 'similarity variable':

$$\eta = \frac{\sigma y}{x} \tag{2}$$

where is $\sigma = 4$.

DOI: 10.1002/fld

2.2.1. Horizontal velocity component, u_x. The horizontal velocity component, u_x, is given by

$$u_x = \mathrm{erf}(\eta) \tag{3}$$

Equation (3) is not a physically realistic velocity profile for a near-wall turbulent flow. Nevertheless, the main goal of including a no-slip condition along the bottom solid wall is satisfied.

2.2.2. Vertical velocity component, u_y. The vertical velocity component, u_y, is computed from the continuity equation in incompressible flow. Thus, the velocity is a divergence free field

$$u_y = \frac{1}{\sigma\sqrt{\pi}}(1 - \mathrm{e}^{-\eta^2}) \tag{4}$$

2.2.3. Pressure, P. The pressure is taken to be

$$C_p = \frac{P}{\rho(U_1)^2} = 0.5\ln(2x - x^2 + 0.25)\ln(4y^3 - 3y^2 + 1.25) \tag{5}$$

2.3. Turbulence quantities for the Spalart & Allmaras one-equation model

The Spalart & Allmaras model uses a dependent variable $\tilde{\nu}$ related to the eddy-viscosity, ν_t, by a damping function f_{v1}. As discussed in [8], it is preferable that a MS in the one-equation models specifies the dependent variable $\tilde{\nu}$ instead of the eddy-viscosity, ν_t. The manufactured ν_t will be deduced from the relationship between ν_t and $\tilde{\nu}$ as follows.

2.3.1. Eddy-viscosity, ν_t. In the Spalart & Allmaras model, [9], ν_t is given by

$$\nu_t = \tilde{\nu} f_{v1} \tag{6}$$

with

$$f_{v1} = \frac{\chi^3}{\chi^3 + c_{v1}^3} \tag{7}$$

and

$$\begin{aligned} \chi &= \frac{\tilde{\nu}}{\nu} \\ c_{v1} &= 7.1 \end{aligned} \tag{8}$$

2.3.2. Specification of the turbulence model-dependent variable, $\tilde{\nu}$. In the MS proposed in [8], $\tilde{\nu}$ is given by

$$\tilde{\nu} = 0.25\tilde{\nu}_{\max}\eta_v^4 \mathrm{e}^{2-\eta_v^2} \tag{9}$$

where

$$\eta_v = \frac{\sigma_v y}{x} \tag{10}$$

$\sigma_v = 2.5\sigma$ and $\tilde{\nu}_{\max}$ is $10^3\nu$.

DOI: 10.1002/fld

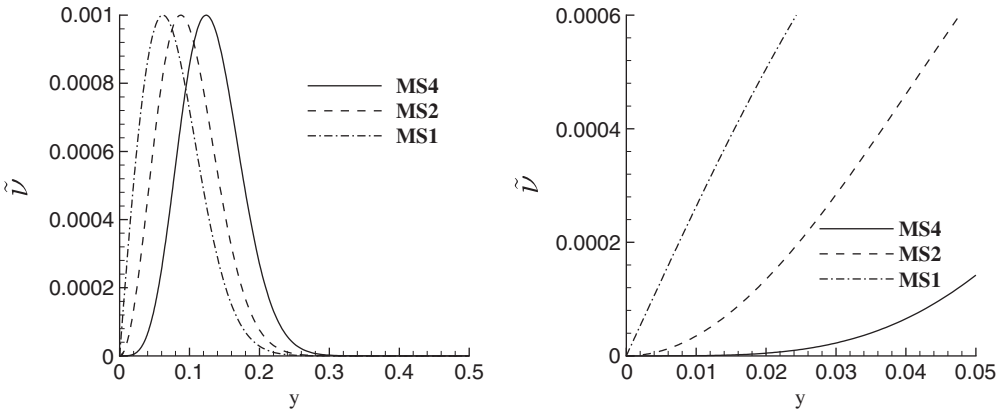

Figure 1. Manufactured profiles of $\tilde{\nu}$ at $x = 0.875$.

In a near-wall turbulent flow, ν_t varies with y^4. This behaviour is not completely reproduced by Equation (10) due to the effect of the damping function, f_{v1}. Furthermore, in the MS this behaviour will not be as local as in a real near-wall turbulent flow. We will refer to this MS as MS4.

To avoid the numerical difficulties imposed by the y^4 dependence of $\tilde{\nu}$ in MS4, an alternative manufactured $\tilde{\nu}$ is proposed. In this MS, $\tilde{\nu}$ is given by

$$\tilde{\nu} = \tilde{\nu}_{\max} \eta_v^2 e^{1-\eta_v^2} \tag{11}$$

Equation (11) is similar to that of the original MS, Equation (9), but in this case $\tilde{\nu}$ depends only on the second power of the wall distance, y^2. Accordingly, we will designate this case by MS2.

A third possibility, denoted by MS1, was also considered for the specification of $\tilde{\nu}$. The proposed function varies linearly with y in the near-wall region and presents the same exponential decay as in the other two MSs

$$\tilde{\nu} = \tilde{\nu}_{\max} \sqrt{2} \eta_v e^{0.5-\eta_v^2} \tag{12}$$

Figure 1 shows the three manufactured profiles of $\tilde{\nu}$ at $x = 0.875$, including a detailed view of the near-wall $\tilde{\nu}$ profiles. The maximum of $\tilde{\nu}$ is identical in the three cases, but it occurs at three different locations: $\eta_v = \sqrt{2}$ for the MS4, $\eta_v = 1$ for the MS2 and $\eta_v = \sqrt{2}/2$ for the MS1.

The three MSs satisfy the wall boundary condition of a near-wall turbulent flow: $\tilde{\nu} = 0$. However, the proposed formulas lead to significant differences in some of the terms of the transport equation for $\tilde{\nu}$. In the Spalart & Allmaras model, dissipation is proportional to the ratio between $\tilde{\nu}$ and y (the distance to the wall), which behaves very differently in the three MSs. In the near-wall region, this ratio is proportional to y^2 for MS4 and to y in MS2. Therefore, dissipation tends to zero at the bottom of the domain in both cases. In the MS1 case, this ratio tends to a constant at the wall. Hence, the turbulent flow solver may exhibit different convergence behaviour for the three MS.

DOI: 10.1002/fld

2.4. Turbulence quantities for the TNT and BSL k–ω two-equation models

For the TNT and BSL versions of the k–ω turbulence model, we have tested five alternative MSs based on different specifications of the eddy-viscosity, ν_t, and the turbulence kinetic energy, k. The specification of the eddy-viscosity is identical to that presented above for $\tilde{\nu}$. However, we have adopted two different strategies for k: use a definition equation of the same type of the one used for $\tilde{\nu}$; or apply Bradshaw's hypothesis for turbulence in equilibrium that states that k is proportional to the product of ν_t by the strain rate, S

$$k = \frac{\nu_t}{0.3} S \tag{13}$$

where

$$S = \left(\frac{\partial u_x}{\partial y} + \frac{\partial u_y}{\partial x} \right) \tag{14}$$

ω is obtained from the eddy-viscosity definition:

$$\omega = \frac{k}{\nu_t} \tag{15}$$

Therefore, when Equation (13) is adopted for the definition of k, ω is given by

$$\omega = \frac{S}{0.3} \tag{16}$$

The main disadvantage of such approach is that it is not representative of the theoretical behaviour of ω near a solid wall. However, this may prove to be a numerical advantage because close to a wall ω varies with y^{-2} and so is singular at the wall whereas equation (16) is not.

Like the MSs for the Spalart & Allmaras model, the MSs proposed for the k–ω model will be designated according to the equations selected for the eddy-viscosity and turbulence kinetic energy definition, as detailed below.

2.4.1. MS4 and MS4B. These two MSs use the same definition of ν_t given by Equation (9) with $\tilde{\nu}$ replaced by ν_t, while $\tilde{\nu}_{\max} \equiv (\nu_t)_{\max}$. The number 4 in their designation refers to the y^4 behaviour. For the MS4, which corresponds to the original MS proposed in [8], k is defined by

$$k = k_{\max} \eta_v^2 \mathrm{e}^{1-\eta_v^2} \tag{17}$$

Close to the bottom of the domain ($y = 0$), i.e. in the near-wall region, k varies with y^2 and the maximum of k occurs closer to the wall than the maximum of ν_t. The proposed value of $k_{\max}$ is 0.01.

With these definitions of ν_t and k, ω is given by

$$\omega = 4 \frac{k_{\max}}{(\nu_t)_{\max}} \mathrm{e}^{-1} \eta_v^{-2} = 4 \frac{k_{\max}}{(\nu_t)_{\max}} \mathrm{e}^{-1} \frac{x^2}{\sigma_v^2 y^2} \tag{18}$$

This distribution of ω is physically realistic in that it behaves as y^{-2} near the wall. Thus, the Ms for ω raises the same problem found in real near-wall turbulent flows: ω goes to infinity at the wall.

DOI: 10.1002/fld

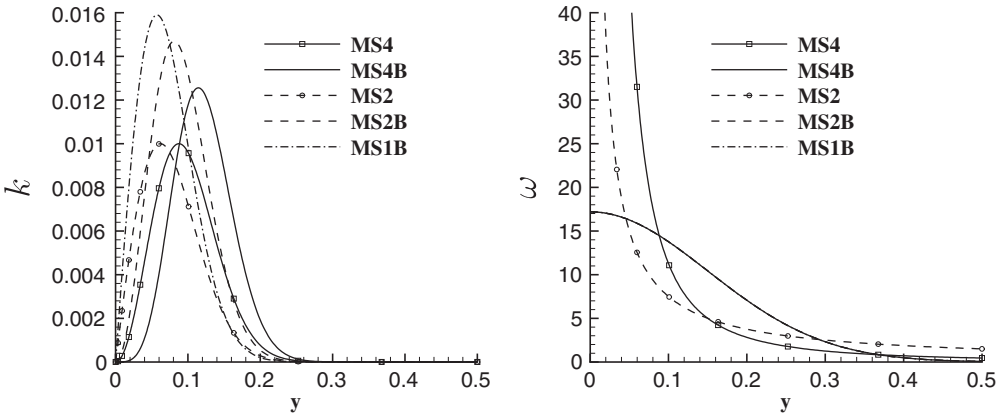

Figure 2. Manufactured profiles of k and ω at $x = 0.875$.

The alternative MS4B is constructed with the same ν_t, but with k given by Equation (13). Therefore, ω is defined by the strain rate and tends to a finite value at the wall. It is interesting to investigate the numerical consequences of this change in the ω boundary condition at the bottom of the domain.

2.4.2. MS2 and MS2B. The MS2 and MS2B are similar to the previous MSs. In both cases, ν_t is defined by Equation (11) with $\tilde{\nu}$ replaced by ν_t. The number 2 in their designation obviously refers to the y^2 behaviour. In the MS2B case, k is given by Bradshaw's equilibrium hypothesis, Equation (13). Therefore, ω is defined by Equation (16).

For the MS2, k is defined to have a linear dependency on y for the near-wall region and an exponential decay in the outer region:

$$k = k_{\max}\sqrt{2}\eta_v \mathrm{e}^{0.5-\eta_v^2} \tag{19}$$

Consequently, ω is given by

$$\omega = \sqrt{2}\frac{k_{\max}}{(\nu_t)_{\max}}\mathrm{e}^{-0.5}\eta_v^{-1} = \sqrt{2}\frac{k_{\max}}{(\nu_t)_{\max}}\mathrm{e}^{-0.5}\frac{x}{\sigma_v y} \tag{20}$$

Just like for MS4, ω goes to infinity at the wall in the MS2. However, ω varies like y^{-1} instead of y^{-2} in the near-wall region.

2.4.3. MS1B. The fifth option tested uses an eddy-viscosity defined by Equation (12) and the turbulence kinetic energy specified from the Bradshaw equilibrium hypothesis, Equation (13). Therefore, ω is identical to that of the MS4B and MS2B cases, Equation (16).

The manufactured eddy-viscosity has the same expression of the manufactured $\tilde{\nu}$ for the Spalart & Allmaras turbulence model (i.e. $\nu_t = \tilde{\nu}$). Therefore, the ν_t profiles at $x = 0.875$ are equal to the $\tilde{\nu}$ profiles plotted in Figure 1. Figure 2 presents the manufactured profiles of k and ω at $x = 0.875$ for the five MSs proposed.

Although the k profiles of the five MSs exhibit similar behaviours, the near-wall variations and the peak values are clearly different for all five MSs. The most significant differences are observed

DOI: 10.1002/fld

for the ω profiles. Bradshaw's equilibrium hypothesis leads to the same ω profile for the MS4B, MS2B and MS1B, which exhibits a nearly constant value in the near-bottom region. On the other hand, the MS4 and MS2 exhibit a vertical asymptote at the wall which may be expected to have some impact on the convergence properties of the numerical solver.

3. NUMERICAL CALCULATIONS OF THE MANUFACTURED SOLUTIONS

This section presents and discusses results obtained with the PARNASSOS turbulent flow solver for the MSs presented in the previous sections. Effects of the MS structure and functional forms of the numerical performance of PARNASSOS are highlighted.

3.1. Flow solver

All calculations were performed with the 2-D finite-difference version of PARNASSOS, [15]; this code solves the steady, incompressible, Reynolds-averaged Navier–Stokes equations using eddy-viscosity turbulence models. The main characteristics of PARNASSOS are:

- The continuity and momentum equations are written in Contravariant form and the momentum balance is computed along the directions of the curvilinear coordinate system.
- A fully collocated arrangement is adopted with the unknowns and the discretization centred at the grid nodes.
- Newton linearization is applied to the convective terms.
- Second-order schemes are applied in the discretization of diffusion and all the coordinate derivatives included in the metric coefficients.
- Velocity derivatives in the continuity equation and the pressure gradient are discretized with third-order schemes using a fixed bias.
- Third-order upwind discretization is applied to the convective terms of the momentum equations.
- The linear system of equations formed by the discretized continuity and momentum equations is solved simultaneously with GMRES, [17], using a coupled ILU preconditioning.
- Under relaxation is applied with a quasi time-derivative term.
- The convective terms of the transport equations of the turbulence quantities are discretized with third-order upwind schemes.
- The linearization procedure of the production and dissipation terms of the turbulence quantities transport equations follows the standard approach, i.e. production is added to the right-hand side and dissipation to the main diagonal.
- The solution of the turbulence quantities transport equations is uncoupled from the solution of the continuity and momentum equations.

The manufactured source term of the momentum equations is computed at each grid node and added to the right-hand side. For the turbulence quantities transport equations the handling of the manufactured source term depends on its sign: a positive term is added to the main diagonal of the system (divided by the dependent variable), whereas a negative term is included in the right-hand side.

DOI: 10.1002/fld

3.2. Grid sets

Although we have tested three different grid sets in our studies [18], in this paper we will focus on the results obtained in a set of Cartesian grids with equidistant grid nodes in the x direction and clustered grid nodes close to the bottom boundary using a one-sided stretching function, [19] (stretching parameter 0.05).

The grid set includes 16 geometrically similar grids covering a grid refinement ratio of 4. The finest grid has 401×401 grid nodes and the coarsest grid 101×101. There are 19×19 physical locations which are common to all grids. This allows to monitor grid convergence of local/point quantities without requiring any sort of interpolation.

3.3. Monitoring the error

Following [3], the error of any flow quantity, ϕ, can be expressed by a power series expansion. Retaining only the lowest order term we have

$$e(\phi) = \phi - \phi_{\mathrm{ms}} \simeq \alpha h_i^p \tag{21}$$

where the subscript $_{\mathrm{ms}}$ identifies the MS, α is a constant, h_i is the typical cell size and p is the convergence rate.

For the present grids,

$$h_i = \frac{1}{NX} = \frac{1}{NY}$$

NX and NY stand for the number of nodes in the x and y directions.

We shall quantify the error in the numerical solution by monitoring both local and global (e.g. friction force on bottom wall) quantities. For a given flow quantity, ϕ, we have computed the root mean square (RMS) of the error of the numerical solution, which is given by

$$\mathrm{RMS}(e(\phi)) = \sqrt{\sum_{i=2}^{NX-1} \sum_{j=2}^{NY-1} \frac{(\phi(j,i) - \phi(j,i)_{\mathrm{ms}})^2}{(NX-2)(NY-2)}} \tag{22}$$

i is the index of the node in the x direction and j is the index of the node in the y direction.

There is no guarantee that the convergence of the flow field is uniform throughout the computational domain (i.e. that p is constant over the whole domain). Hence, we have also analysed the error at 8 fixed locations of the grid set. Their i and j indices are given in Table I, together with their x and y coordinates.

In the results presented in the remainder of this section, the observed order of accuracy, p, and the constant α are determined with a least-squares approach, [20]. The fits plotted in the figures are obtained with the data of the 11 finest grids of each set, i.e. the grids with at least 201×201 grid nodes, covering a grid refinement ratio of 2. However, we have also checked the dependence of the observed order of accuracy on the selected grids. The observed order of accuracy is estimated for different groupings of grids, which must present a grid refinement ratio between the finest and coarsest grid, $r_{i1} = h_i / h_1$, of at least 1.3. This is an important check, because it indicates whether the data obtained in the finest grids are in the so-called 'asymptotic range'.

In all calculations presented below, the iterative error was reduced to machine accuracy and the calculations were performed with 15-digits precision. Therefore, the computed errors are mainly a consequence of the discretization error.

DOI: 10.1002/fld

Table I. Coordinates of the 8 selected locations to monitor the convergence of the numerical solution with the grid refinement ratio.

	i	j	x	$y \times 10^{+3}$
P1	$1+2(NX-1)/20$	$1+(NY-1)/20$	0.55	1.43
P2	$1+4(NX-1)/20$	$1+2(NY-1)/20$	0.60	3.30
P3	$1+6(NX-1)/20$	$1+3(NY-1)/20$	0.65	5.73
P4	$1+8(NX-1)/20$	$1+4(NY-1)/20$	0.70	8.89
P5	$1+10(NX-1)/20$	$1+5(NY-1)/20$	0.75	13.0
P6	$1+12(NX-1)/20$	$1+6(NY-1)/20$	0.80	18.3
P7	$1+14(NX-1)/20$	$1+7(NY-1)/20$	0.85	25.2
P8	$1+16(NX-1)/20$	$1+8(NY-1)/20$	0.90	34.0

3.4. Calculation of the eddy-viscosity field with the manufactured velocity field

The first exercise performed with the proposed MSs was to solve the turbulence transport equations using the manufactured velocity field. It is important to emphasize that the velocity field is identical for all the MS tested. Therefore, any change in convergence properties can readily and formally be attributed to the solution of the turbulence model transport equations.

Dirichlet boundary conditions were applied for the turbulence quantities at the four boundaries of the computational domain. This is straightforward for most of the turbulence quantities. The dependent variable of the one-equation model, $\tilde{\nu}$, the turbulence kinetic energy, k, and ω for the MS4B, MS2B and MS1B are all trivial to set using the MS. However, for the MS4 and MS2 ω goes to infinity at the bottom of the computational domain. This is a common problem with $k-\omega$ models in near-wall turbulent flows. To avoid any influence of the boundary value of ω, we have fixed ω on the first two layers of grid nodes away from the bottom ($j=2$ and 3) using the MS. This is fairly standard practice for the k–ω model, [21].

In PARNASSOS, there are two layers of virtual grid points at each boundary of the computational domain. They guarantee that the stencil of the third-order schemes can be maintained near and at the boundaries of the computational domain. In the present calculations, we have filled in these virtual layers using quadratic extrapolation based on the boundary node and its two closest neighbours, i.e. the MS is only specified at the boundaries of the computational domain.

3.4.1. Spalart & Allmaras one-equation model. The convergence of the RMS error of $\tilde{\nu}$ as a function of the grid refinement ratio is illustrated in Figure 3 for the MS4, MS2 and MS1. The observed order of accuracy at the 8 selected locations of each MS is given in Tables II–IV, which include also p for the RMS error. These results show that the convergence properties of $\tilde{\nu}$ are different for the three MSs. We make the following observations:

- The MS2 is the only one exhibiting the expected behaviour, with a well-established order of accuracy for the RMS error equal to the theoretical order of the method, and a vanishing error for the extrapolation to zero mesh size (see Figure 3). Furthermore, the p of $\tilde{\nu}$ shows a consistent behaviour at all selected locations, and has a value close to the theoretical order of the method (see Table III).
- For MS4, the RMS error of $\tilde{\nu}$ converges with an unexpected first-order accuracy and the value of p for the RMS error is nearly independent of the group of grids selected. Furthermore,

DOI: 10.1002/fld

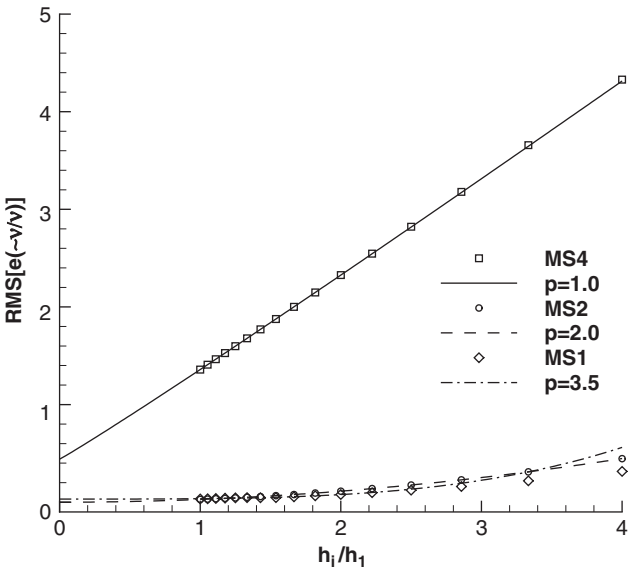

Figure 3. Grid convergence of RMS error of $\tilde{\nu}$. Spalart & Allmaras model with the velocity specified from MS.

Table II. Observed order of accuracy of $\tilde{\nu}$ at the 8 selected locations for the MS4.

Grids	r_{i1}	P1	P2	P3	P4	P5	P6	P7	P8	RMS
1–6	1.33	2.0	2.0	2.1	2.0	2.1	0.7	2.0	2.0	1.0
1–7	1.43	2.0	2.0	2.1	2.0	2.1	0.5	2.0	2.0	1.0
1–8	1.54	2.0	2.0	2.1	2.0	2.1	0.2	2.0	2.1	1.0
1–9	1.67	2.0	2.0	2.1	2.0	2.1	0.0	2.0	2.1	1.0
1–10	1.82	2.0	2.0	2.1	2.0	2.1	0.0	2.0	2.1	1.0
1–11	2.00	2.0	2.0	2.2	2.0	2.1	0.0	2.0	2.1	1.0
1–12	2.22	2.0	2.0	2.2	2.0	2.1	0.0	2.0	2.1	1.0
1–13	2.50	2.0	2.1	2.2	2.0	2.1	—	2.0	2.1	1.0
1–14	2.86	2.0	2.1	2.3	1.9	2.1	—	2.0	2.1	1.1
1–15	3.33	2.0	2.1	2.3	1.9	2.0	7.4	2.0	2.1	1.1
1–16	4.00	2.0	2.1	2.4	1.9	2.0	5.9	2.0	2.1	1.0

Spalart & Allmaras model using the velocity specified from the MS.

the level of the error is substantially larger than for MS2 and MS1 cases and the extrapolated value to zero cell size is inconsistent. However, 7 of the 8 (the exception is P6) selected locations exhibit a well-established order of accuracy, which is close to the theoretical order of the method. Therefore, one concludes that the convergence properties of $\tilde{\nu}$ are dependent on the selected location.

- The MS1 exhibits a RMS error similar to that of MS2 (Table IV). However, there is no consistency in the observed order of accuracy of the RMS error, which shows a significant

DOI: 10.1002/fld

Table III. Observed order of accuracy of $\tilde{\nu}$ at the 8 selected locations for the MS2.

Grids	r_{i1}	P1	P2	P3	P4	P5	P6	P7	P8	RMS
1–6	1.33	1.8	2.0	2.0	2.1	2.1	2.1	2.1	2.2	2.0
1–7	1.43	1.9	2.0	2.0	2.1	2.1	2.1	2.1	2.2	2.0
1–8	1.54	2.1	2.0	2.0	2.1	2.1	2.1	2.1	2.2	2.0
1–9	1.67	1.9	2.0	2.0	2.1	2.1	2.1	2.1	2.2	2.0
1–10	1.82	1.8	2.0	2.0	2.1	2.1	2.2	2.2	2.2	2.0
1–11	2.00	2.0	2.0	2.0	2.1	2.1	2.2	2.2	2.2	2.0
1–12	2.22	1.8	2.0	2.0	2.1	2.2	2.2	2.2	2.2	2.0
1–13	2.50	1.7	2.0	2.0	2.1	2.2	2.2	2.2	2.2	2.0
1–14	2.86	1.9	2.0	2.1	2.1	2.2	2.2	2.2	2.2	2.0
1–15	3.33	1.7	2.0	2.1	2.1	2.2	2.2	2.2	2.3	2.0
1–16	4.00	1.6	2.1	2.1	2.1	2.2	2.2	2.2	2.3	2.0

Spalart & Allmaras model using the velocity specified from the MS.

Table IV. Observed order of accuracy of $\tilde{\nu}$ at the 8 selected locations for the MS1.

Grids	r_{i1}	P1	P2	P3	P4	P5	P6	P7	P8	RMS
1–6	1.33	2.0	2.0	2.0	2.0	2.0	2.0	2.0	2.0	—
1–7	1.43	2.0	2.0	2.0	2.0	2.0	2.0	2.1	2.0	—
1–8	1.54	2.0	2.0	2.0	2.0	2.0	2.0	2.1	1.9	—
1–9	1.67	2.0	2.0	2.0	2.0	2.0	2.0	2.1	1.9	—
1–10	1.82	2.0	2.0	2.0	2.0	2.0	2.0	2.1	1.9	2.5
1–11	2.00	2.0	2.0	2.0	2.0	2.0	2.0	2.1	1.9	3.5
1–12	2.22	2.0	2.0	2.0	2.0	2.0	2.0	2.1	1.9	3.4
1–13	2.50	2.0	2.0	2.0	2.0	2.0	2.0	2.1	1.9	3.0
1–14	2.86	2.0	2.0	2.0	2.0	2.0	2.0	2.1	1.9	2.7
1–15	3.33	2.0	2.0	2.0	2.0	2.0	2.0	2.1	1.9	2.5
1–16	4.00	2.0	2.0	2.0	2.0	2.0	2.0	2.1	1.9	2.3

Spalart & Allmaras model using the velocity specified from the MS.

influence of the groups of grids selected. Furthermore, as for MS4, the extrapolation to zero cell size does not indicate a vanishing error. On the other hand, the observed p at the 8 selected locations is rather consistent and close to the theoretical order of the method. Therefore, as for MS4, the convergence properties of $\tilde{\nu}$ are dependent on the selected location.

These awkward results show that the construction of a MS for code verification of the Spalart & Allmaras eddy-viscosity turbulence model is not trivial. However, they are perhaps not completely surprising, because all the terms of the $\tilde{\nu}$ transport equation are non-linear with the exception of convection which, in the present context of a fixed velocity field, is a linear term.

In MS4, the numerical difficulties are caused by the near-wall behaviour of $\tilde{\nu}$. Figure 4 presents the $\tilde{\nu}$ profiles at $x = 0.875$ obtained for MS4 and MS2 on 4 grids. In this plot we have included an extra level of grid refinement, 801×801. The data plotted for the MS4 in Figure 4 show an oscillation in the calculated $\tilde{\nu}$ profiles in the near-wall region that disappears very slowly with grid

DOI: 10.1002/fld

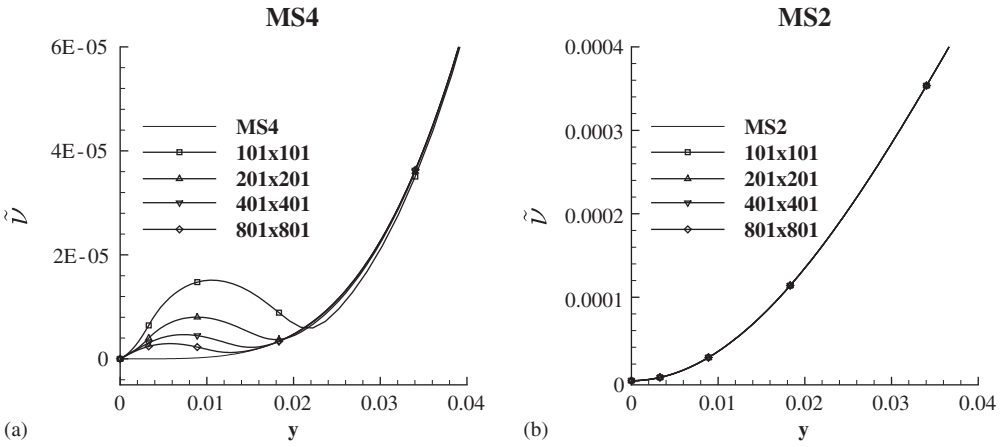

Figure 4. $\tilde{\nu}$ profiles at $x = 0.875$ for the MS4 and MS2. Spalart & Allmaras model using the velocity specified from the MS.

refinement. This oscillation increases with the distance from the inflow boundary, i.e. a similar comparison for $x < 0.875$ exhibits smaller differences between MS4 and the profiles from the 4 grids. However, the MS2 case in which $\tilde{\nu}$ varies only with y^2 shows graphically coincident lines for the four grids on Figure 4b.

The origin of the problems for the MS1 must be different because $\tilde{\nu}$ has a simpler near-wall behaviour than in MS2. In order to investigate the origin of the problem, we have computed the convergence of the error of the four terms in the $\tilde{\nu}$ transport equation: convection, diffusion, production and dissipation. Furthermore, we have performed an extra set of calculations for the MS1 where production and dissipation are taken exactly from the MS. We will designate this set of results by $\mathrm{MS1_{ms}}$.

The RMS error of the four terms of the $\tilde{\nu}$ transport equation are presented in Figure 5 as a function of the grid refinement ratio. While we have used the manufactured production and dissipation terms in the $\mathrm{MS1_{ms}}$ solution, we still monitor the error of these terms in the converged solutions.

The data plotted in Figure 5 show several interesting features:

- The two terms that involve derivatives of $\tilde{\nu}$ exhibit the largest errors for the MS4. This is a consequence of the oscillation of the $\tilde{\nu}$ profiles seen in Figure 4.
- For MS1, the RMS error of dissipation, production and diffusion obtained in the six finest grids are outside the plotted region. These are the three terms which involve $\tilde{\nu}$, whereas convection includes only derivatives of $\tilde{\nu}$. These results explain the difficulties to obtain the observed order of accuracy of the RMS of the error of $\tilde{\nu}$ for the MS1 solution.
- On the other hand, the RMS error of the four terms of the $\tilde{\nu}$ transport equation in the $\mathrm{MS1_{ms}}$ case show that the problems originated with the dissipation term, which presents a much larger error level than the other three terms. As we have mentioned previously, unlike the other two MSs, MS1 has a dissipation term that does not go to zero at the wall. This constant dissipation term in the near-wall region must be more difficult to compute accurately when the near-wall grid line distance is reduced.

DOI: 10.1002/fld

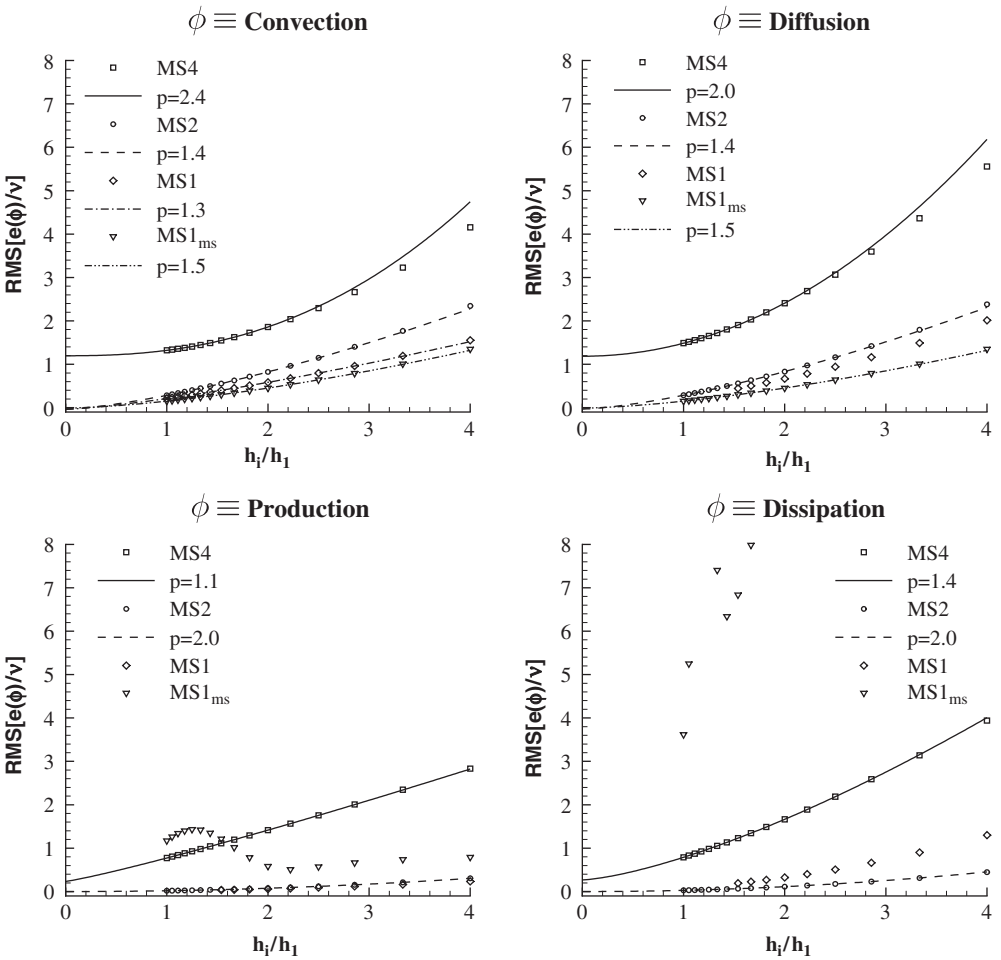

Figure 5. Grid convergence of RMS error of the terms in the $\tilde{\nu}$ transport equation. Spalart & Allmaras model using the velocity specified from MS.

- Although the convergence of the four terms of the $\tilde{\nu}$ transport equation is perfectly smooth for MS2, it is interesting to note that convection and diffusion do not converge with the same second-order accuracy as $\tilde{\nu}$.

In practical turbulent flow calculations the quantity of interest is not $\tilde{\nu}$ but the eddy-viscosity, ν_t. Although the two quantities are identical in a substantial part of the computational domain, the damping function f_{v1} may influence the convergence properties of ν_t. One must not forget that f_{v1} is a non-linear function of $\tilde{\nu}$. Figure 6 presents the convergence with the grid refinement of the RMS error of ν_t to the left and of $\tilde{\nu}$ and ν_t at the location P5 for the MS4 to the right. Unfortunately, f_{v1} is 1 or close to 1 for the MS2 and MS1 at the selected locations and so ν_t coincides with $\tilde{\nu}$ at these locations.

DOI: 10.1002/fld

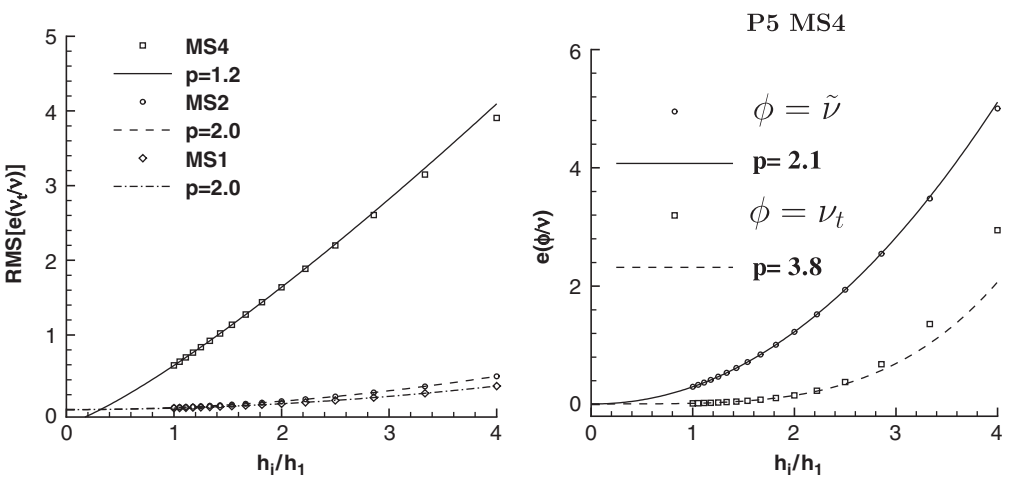

Figure 6. Grid convergence of the RMS error of v_t and errors of $\tilde{v}$ and v_t at the location P5. Spalart & Allmaras model using the velocity specified from MS.

The RMS error of v_t exhibits convergence properties which are not the same as those of $\tilde{v}$ for MS4 and MS1. In MS4 case, the observed order of accuracy for v_t is larger than that of $\tilde{v}$. This is a consequence of the behaviour of the solution in the region where f_{v1} is smaller than 1. As illustrated in Figure 6, the convergence of v_t at the location P5 is affected by the value of f_{v1}, which causes an artificially high value of p in the case of v_t. On the other hand, the problematic region of the MS1 is close to the location where the damping function tends to zero and so the convergence of the RMS error of v_t does not exhibit any of the problems discussed previously for $\tilde{v}$ on Figures 4 and 5.

These results show that the damping functions in the turbulence model may affect the convergence properties of the various turbulence quantities. Furthermore, they illustrate once more the difficulties to manufacture solutions for code verification of the Spalart & Allmaras model, because the effects of the damping function are different in the three solutions tested.

3.4.2. TNT and BSL k–ω two-equation models. The two dependent variables of these turbulence models are k and ω. The main difference between the two versions of the k–ω model tested is the coefficient that multiplies the cross-diffusion term. The TNT version includes an on/off switch, whereas the BSL version includes a blending function, F_1, which is dependent on y, k and ω.

Surprisingly, we had numerical difficulties to converge the BSL model for MS2B, which we did not encounter with the TNT version. With the BSL model in the MS2B, it was impossible to reduce the iterative error to machine accuracy. Even so, the convergence stagnates at a level where it is possible to neglect the iterative error, [22]. The problems originate from the determination of the blending function, F_1, and the cross-diffusion term. Therefore, to clarify issues, we have performed calculations with F_1 and the cross-diffusion term taken from the MS for the BSL k–ω model, which we will designate by $\mathrm{MS2B_{ms}}$. With such an approach it was easy to reduce the iterative error to machine zero.

DOI: 10.1002/fld

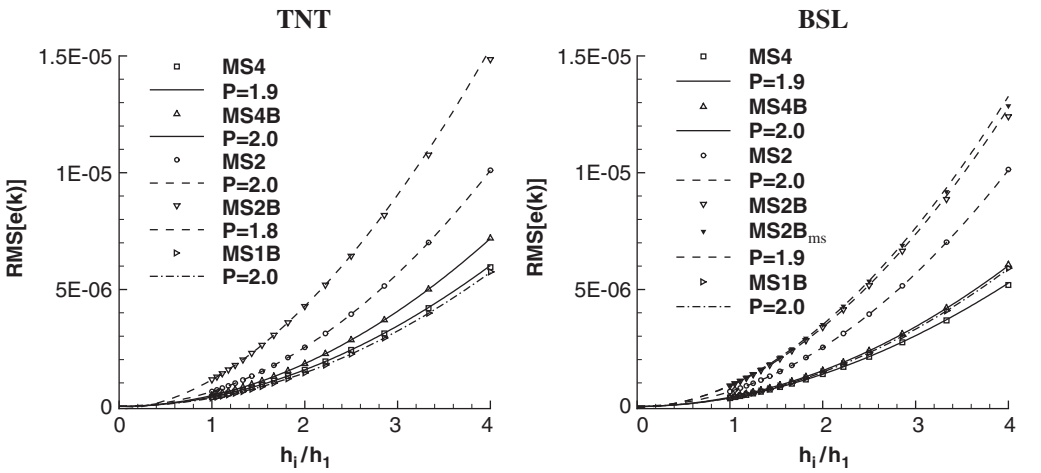

Figure 7. Grid convergence of the RMS error of k. TNT and BSL k–ω models using the velocity specified from MS.

Figure 7 presents the RMS error of k for the TNT and BSL versions of the k–ω model and the five MSs as a function of the grid refinement ratio. We observe the following:

- The convergence of the RMS error of k for the five MSs yields an observed order of accuracy (1.8–2) very close to the theoretical order (2) of the method for the two versions of the k–ω model.
- For a fixed grid refinement level, the errors of MS2B and MS4B are larger than those of MS2 and MS4, which have exactly the same eddy-viscosity field.
- The largest errors are obtained for the MSs where the eddy-viscosity varies as y^2 in the near-wall region; the smallest errors occur for the case of a linear dependence of ν_t on y. This is a somehow unexpected result, because one would think that the highest order specification of k, MS4B, leads to the largest errors.
- The convergence of k for the MS2B and MS2B$_{\text{ms}}$ calculations with the BSL model are almost identical, because the k equation is dealt with in the same manner in both cases.

Figure 8 presents the convergence of the RMS error of ω with the grid refinement ratio for the five MSs with the two versions of the k–ω model tested. We recall that the manufactured ω is the same for MS4B, MS2B and MS1B. Furthermore, ω has a finite value at the wall for these three MSs while it tends to infinity for the MS4 and MS2. The convergence properties of ω are clearly more affected by the MS selected than the convergence properties observed for k. Due to the different orders of the RMS error of ω for the five MS, Figure 8 includes separate graphs for the MS4B, MS2B and MS1B.

- A careless observation of the plots of Figure 8 may lead to the conclusion that the solution is diverging for MS4 and MS2. This would be an inconsistent conclusion because the k solution converges for all MSs. Further inspection indicates that this behaviour of the RMS error of ω is a consequence of the ω boundary condition applied at the wall. The RMS error grows with the grid refinement for the MS4 and MS2 due to the reduction of the distance of the grid

DOI: 10.1002/fld

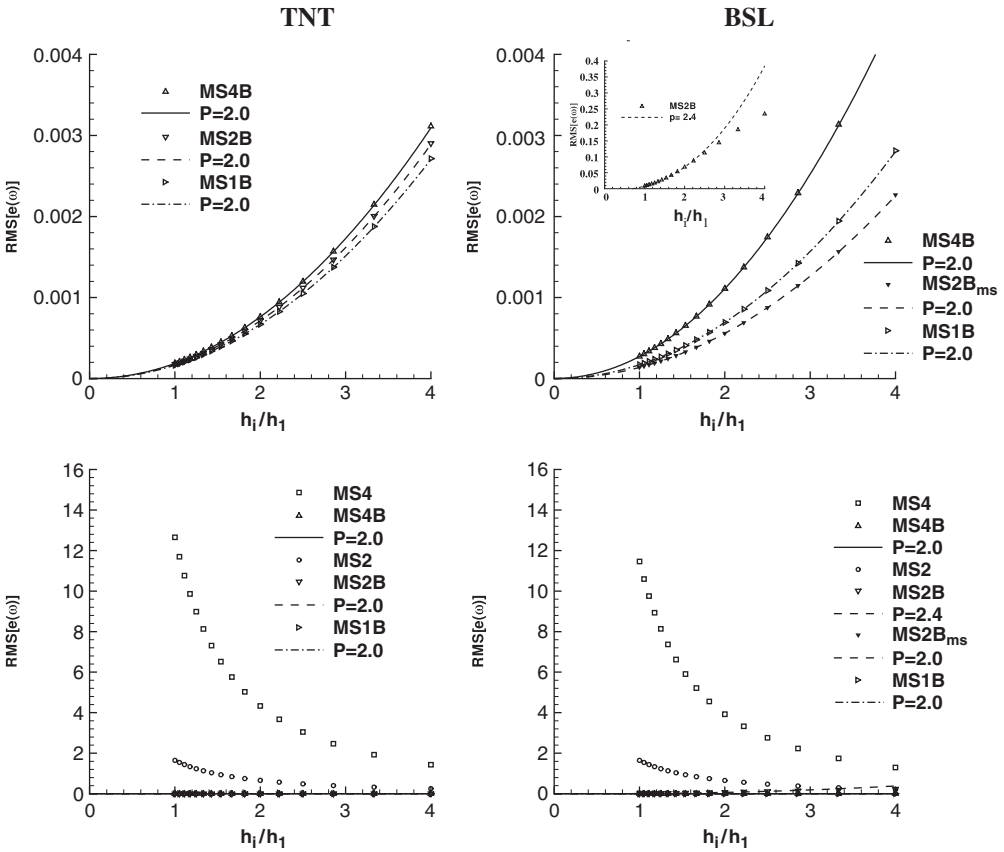

Figure 8. Grid convergence of the RMS error of ω. TNT and BSL k–ω models using the velocity specified from MS.

nodes to the wall. Logically, the effect is stronger for MS4 (at the first grid node away from the wall $\omega \sim y^{-2}$) than for the MS2 (at the first grid node away from the wall $\omega \sim y^{-1}$).

- As expected, the convergence of ω for the MS4B, MS2B and MS1B is very similar for the TNT version of the model, exhibiting an observed order of accuracy equal to the theoretical order of the method for the three cases.
- On the other hand, the BSL version of the model leads to significant differences in the convergence properties of ω for the MS4B, MS2B and MS1B.
  - — The MS2B leads to an RMS error two orders of magnitude larger than those of MS4B and MS1B. The calculations performed with the blending function, F_1, and the cross-diffusion term taken from the MS, $\mathrm{MS2B_{ms}}$, exhibit the same observed theoretical convergence as found with MS4B and MS1B ($p = 2$).
  - — The differences between the error levels of the MS4B and MS1B are significantly larger for the BSL version than for the TNT k–ω model.

DOI: 10.1002/fld

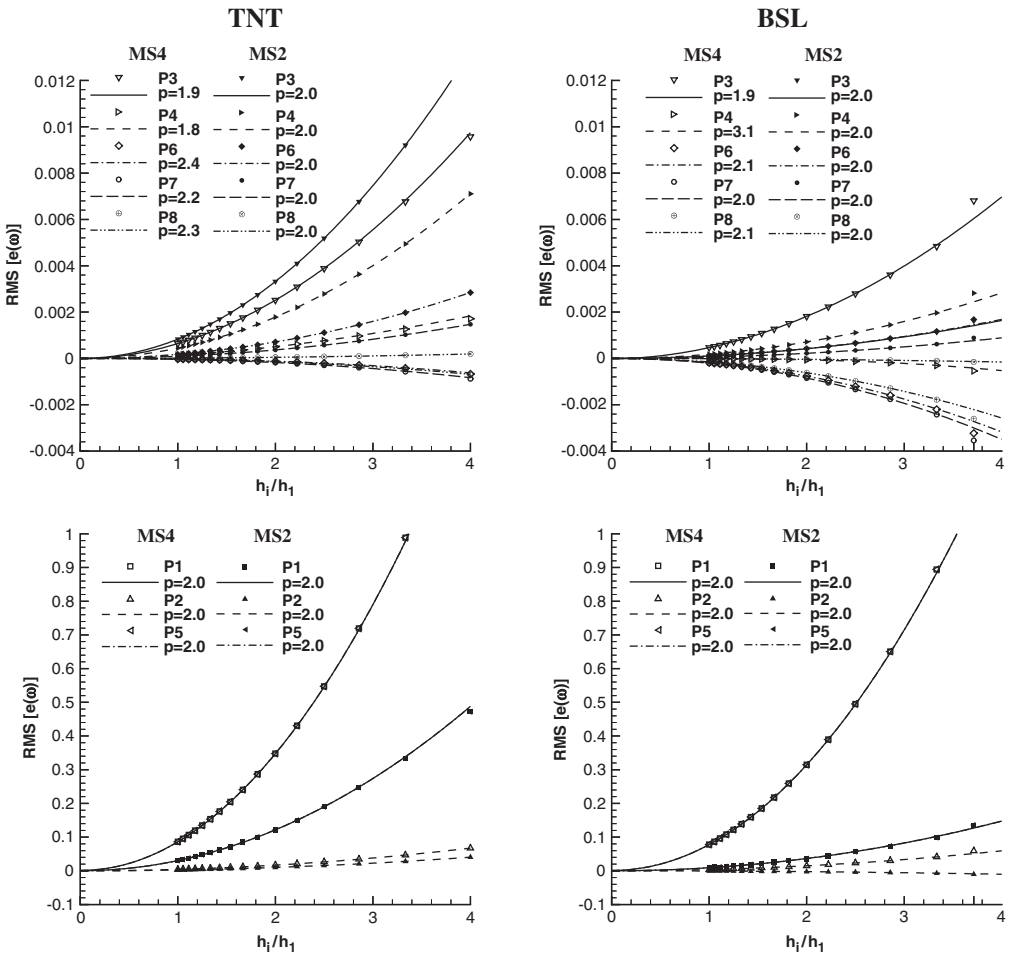

Figure 9. Grid convergence of the error of ω at the 8 selected locations. TNT and BSL k–ω models using the velocity specified from MS.

To illustrate that the large values of the RMS error obtained for the MS4 and MS2 are a consequence of a local phenomena, namely the singular boundary condition, Figure 9 presents the convergence of the error of ω at the 8 selected locations for the two versions of the k–ω model tested. Note that 5 points exhibit small errors (P3, P4, P6, P7, P8) and three others show larger errors (P1, P2, P5). For clarity the two groups of points are plotted on separate graphs. The data plotted in Figure 9 show that:

- Although the results of the two versions of the k–ω model are not exactly equal, the trends observed in the two models are the same.
- Most of the locations exhibit an observed order of accuracy equal to 2. All extrapolations performed with the least-squares approach applied to the 11 finest grids indicate a vanishing error for zero cell size.

DOI: 10.1002/fld

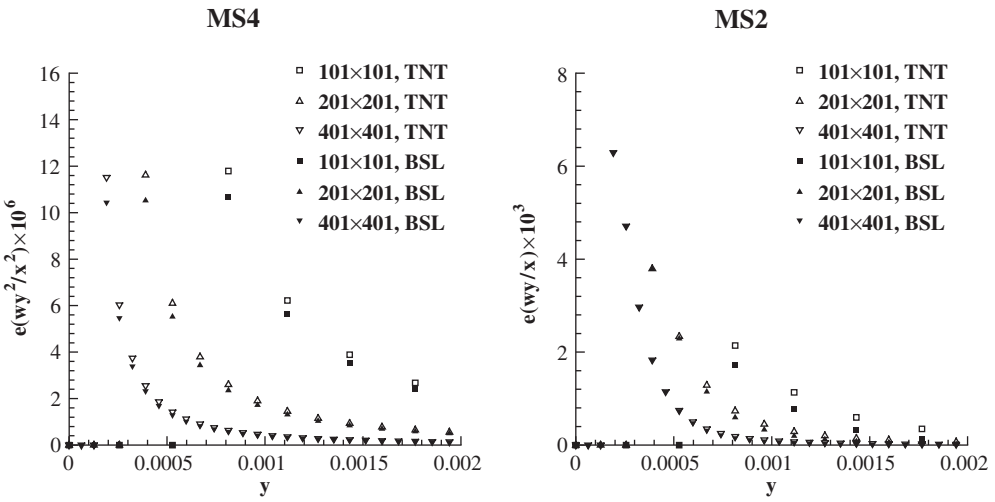

Figure 10. Error of ω in the near-wall region at $x = 0.875$. Manufactured velocity field.

- There are two locations, P1 and P5, that exhibit error levels two orders of magnitude larger than those obtained at the five other locations. At point P2, the error level is smaller than in P1 and P5, but clearly larger than for the remaining locations.

The problems originating at the wall boundary condition of ω in the MS4 and MS2 are illustrated in Figure 10. The error of the ω profiles at $x = 0.875$ is plotted in the near-wall region. We have computed the error of $\omega y^2/x^2$ for MS4 and the error of $\omega y/x$ for MS2, which are both constant values for the complete computational domain (see Equations (18) and (20)). The behaviour of the error for the MS4, where ω varies with y^{-2}, is exactly the same as we have observed for the k–ω model in simple flat plate boundary-layer flows, [23]: the error level at the first grid node off the wall where ω is computed from its transport equation is almost independent of the grid refinement level; the error decays rapidly with the increase of the distance to the 'wall'.

On the other hand, for MS2, for which ω behaves as y^{-1}, ω shows a substantially smaller error than MS4. In this case, the error level at the first grid node where the ω transport equation is solved increases with the grid refinement.

In order to understand the differing behaviours of the two versions of the k–ω model tested, Figure 11 presents the cross-diffusion term of the ω transport equation at $x = 0.875$ for the five MSs. It is clear that the cross-diffusion term generated by the manufactured k and ω behaves in a much better manner in the TNT formulation than in the BSL version.

In the BSL version, there are MSs where the cross-diffusion profiles present kinks, due to the definition of the blending function, F_1, as illustrated in Figure 12. In MS4 the cross-diffusion term tends to a constant value at the wall, $y = 0$, whereas for the MS2 it goes to infinity. This being said, none of these MSs caused numerical convergence problems with the BSL version. The 'problematic' MS is MS2B, which exhibits a small oscillation (which is hardly visible in Figure 11) close to $y = 0.05$ before it grows to positive values. As an example of the difficulties to manufacture solutions for code verification of eddy-viscosity turbulence models, Figure 12 presents the profiles of the blending function of the BSL model, F_1, at $x = 0.875$ for the five MSs. There

DOI: 10.1002/fld

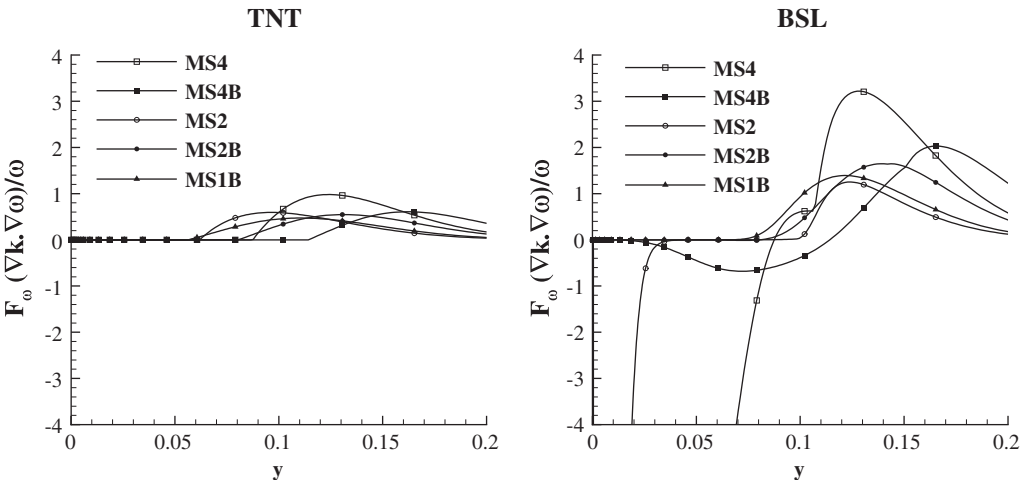

Figure 11. Profiles of the cross-diffusion term of the ω transport equation of the TNT and BSL k–ω models at $x = 0.875$.

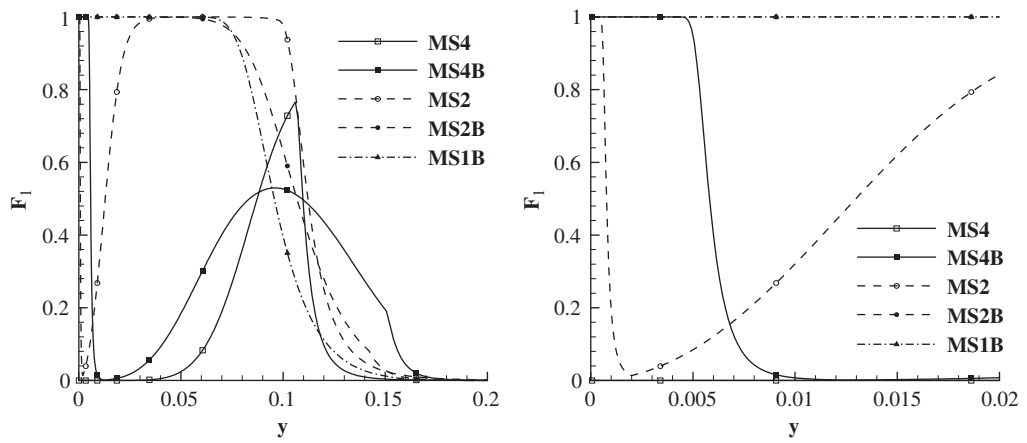

Figure 12. Profiles of the blending function, F_1, of the BSL k–ω model at $x = 0.875$.

are MSs where F_1 does not reach 1 and others where the profiles have kinks. Nevertheless, none of these MSs led to numerical convergence problems. Amazingly, the 'problematic' MS is one of the few that shows the expected behaviour of F_1, with a constant value of 1 in the near-wall region and a rapid decay to zero in the outer region.

As for the Spalart & Allmaras model, the dependent variables of the k–ω turbulence model are not the quantity used in the Reynolds-averaged momentum equations. Therefore, it is important to check the convergence properties of the eddy-viscosity, v_t, which in these two versions of the k–ω model is obtained from the ratio of k and ω.

DOI: 10.1002/fld

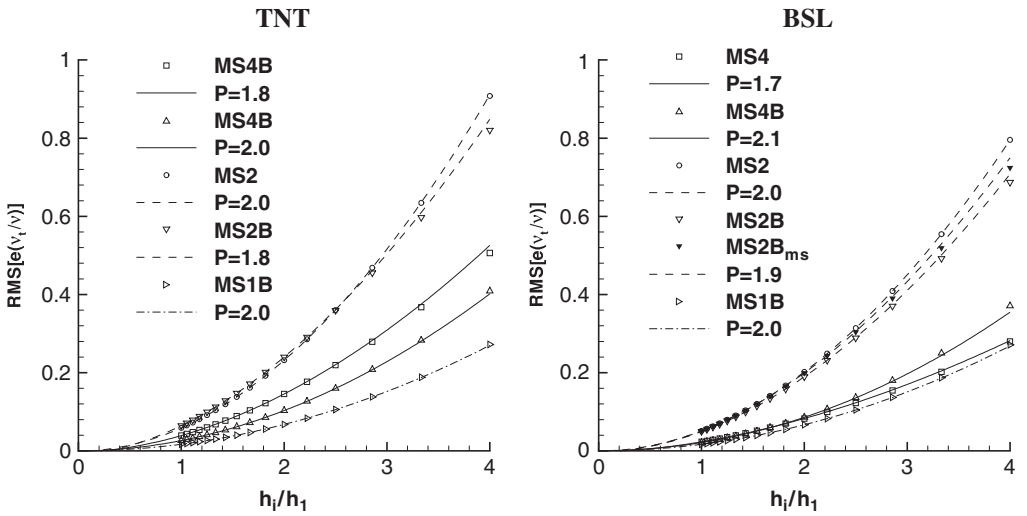

Figure 13. Grid convergence of the RMS error of v_t. TNT and BSL k–ω models using the velocity specified from MS.

Figure 13 presents the convergence of the RMS error of v_t as a function of the grid refinement ratio for the TNT and BSL k–ω models for the five MSs. The observed order of accuracy is close to the theoretical order of the method for all the cases. There are a few details that should be highlighted:

- The largest error levels are obtained for the MS2, which is not equivalent to the trends observed for k and ω. On the other hand, the lowest level of the error is consistently observed for the MS1B.
- In the BSL method, the convergence of the MS2B and MS2B_{ms} does not reflect the significant difference between the two fields of ω.
- The error levels of the MS4 and MS2 are larger than for the MS4B and MS2B, which is in agreement with the ω solution but with the opposite trend observed for the k convergence properties, where the RMS error of MS4 and MS2 are smaller than those of MS4B and MS2B.

3.5. Calculation of the complete flow field

The calculation of the complete flow field was performed with boundary conditions typical of a boundary-layer flow. The following Dirichlet boundary conditions were applied using the MS values: u_x and u_y at the bottom wall; u_x and u_y at the inlet boundary; u_x and C_p at the top boundary. At the outlet boundary, the derivatives of u_x, u_y and C_p with respect to x were set equal to the values defined by the MSs.

At the top boundary, there is no boundary condition for u_y because the continuity equation includes only first derivatives. Therefore, u_y is obtained from mass conservation at the top boundary. At the inlet and wall boundaries, C_p does not require any boundary conditions (the momentum

DOI: 10.1002/fld

equations include only first-order derivatives of p). At these boundaries, C_p can be extrapolated from the interior of the domain or calculated from the local solution of the momentum equations. However, in the present calculations we have just made the first derivative of the pressure equal to the value of the MSs.

For turbulence quantities, the boundary conditions at the inlet, bottom and top boundaries are the same as in the previous exercise. At the outlet boundary, the derivative of any turbulence quantity with respect to x was set equal to the exact value of the corresponding MS.

The two layers of virtual grid nodes were filled in using quadratic extrapolation based on the boundary node and its two closest neighbours for all the flow variables.

In this second exercise, we will focus our attention on the convergence of the horizontal velocity component, u_x, eddy-viscosity, ν_t, and on the 'friction' resistance coefficient at the bottom of the computational domain , C_{D}, defined by

$$C_{\mathrm{D}} = \frac{4}{U_1^2} \int_{0.5}^{1} \nu \left(\frac{\partial u_x}{\partial y} \right)_{y=0} \mathrm{d}x \tag{23}$$

which is evaluated using a second-order accurate numerical integration scheme. The exact value of the 'friction' resistance coefficient is

$$C_{\mathrm{D}} = \frac{16}{\sqrt{\pi}} \ln(2) \nu$$

To provide more insight into the origin of any unexpected results, we will also include results obtained in the calculation of the flow field using the eddy-viscosity from MS. We will refer to these results with the subscript $_{\nu \mathrm{ms}}$.

3.5.1. Spalart & Allmaras one-equation model. The numerical difficulties observed in the previous exercise for the MS1 became worse when the velocity field is also computed as part of the solution. Therefore, we have only computed the complete flow field for the MS4 and MS2.

Figure 14 presents the RMS error of u_x and C_{D} as a function of the grid refinement level. The results obtained using the manufactured eddy-viscosity field exhibit a well-established observed order of accuracy equal to the theoretical order of the method. However, significantly different trends were found in the complete flow field calculations:

- As expected, the MS4 exhibits a poor convergence of C_{D} with the grid refinement ratio. In the previous section, this behaviour was traced to the wall region. The convergence of u_x is also affected by the difficulties observed in the numerical determination of the eddy-viscosity field.
- In the MS2, the numerical calculation of the eddy-viscosity field with a frozen velocity field showed the expected behaviour. However, for the complete flow field calculations the observed order of accuracy obtained for the RMS error of u_x and for C_{D} is below the theoretical order of the method. Fortunately, the extrapolations to zero grid size are consistent, which is not the case of the RMS of u_x for the MS4.

The convergence of the RMS error of ν_t as a function of the grid refinement ratio is presented in Figure 15. To allow an easy comparison with the results from the previous exercise, the plot also includes the results obtained with a frozen velocity field, designated by the subscript $_{e1}$.

DOI: 10.1002/fld

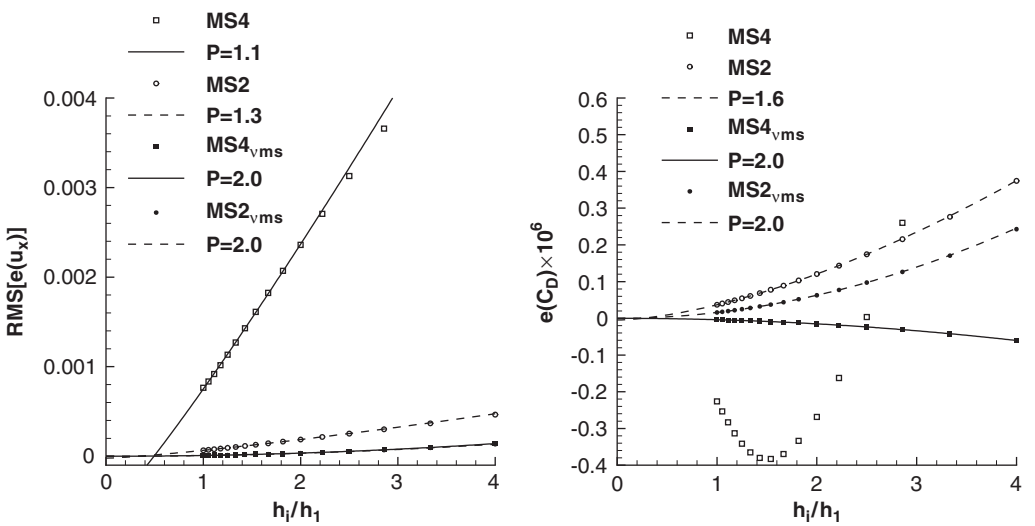

Figure 14. Grid convergence of the RMS of the error of the horizontal velocity component, u_x, and of friction resistance coefficient at the wall, C_D. Spalart & Allmaras model.

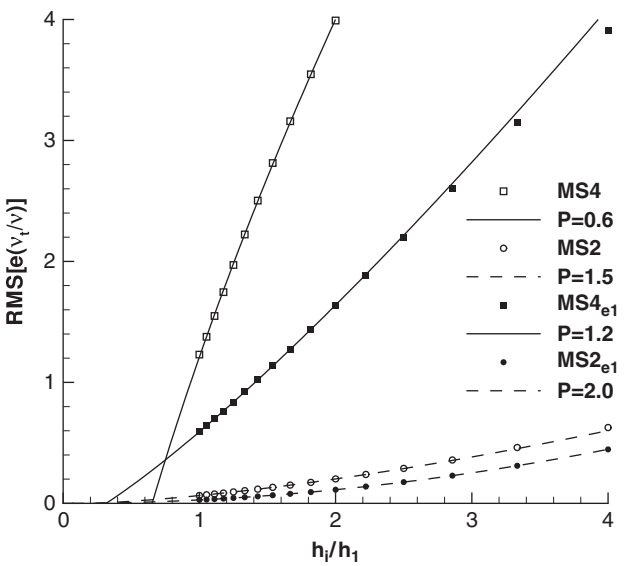

Figure 15. Grid convergence of the RMS error of the eddy viscosity. Spalart & Allmaras model.

The data plotted in Figure 15 show that the observed order of accuracy for v_t is smaller in the complete flow field calculation than in the previous exercise where the velocity field is taken from the MS. However, the simple solution of the turbulence model transport equation is sufficient to identify the problems observed in the complete flow field calculation.

DOI: 10.1002/fld

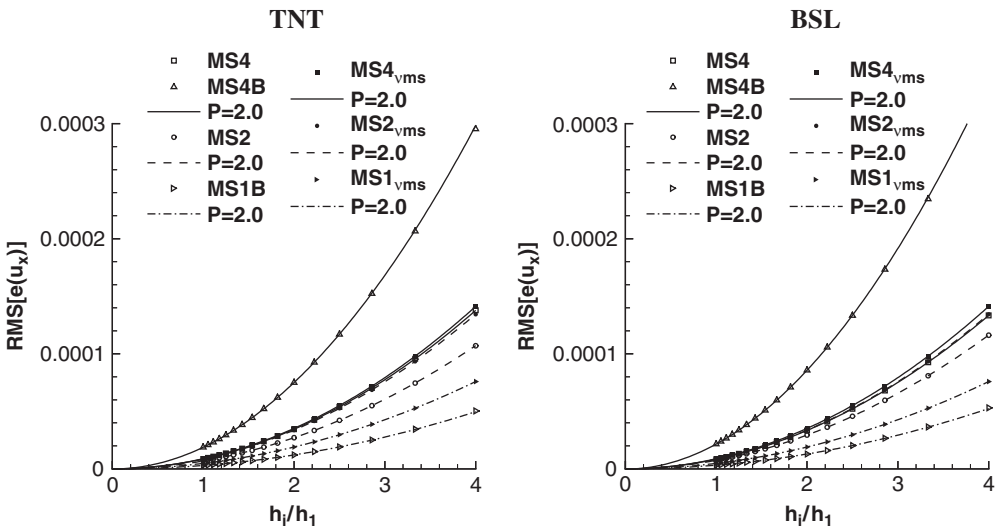

Figure 16. Grid convergence of the RMS error of the horizontal velocity component, u_x. TNT and BSL k–ω models.

3.5.2. TNT and BSL k–ω two-equation models. With the two versions of the k–ω model, numerical difficulties were encountered when solving for MS2B. The problems observed for the previous exercise with the manufactured velocity field in the BSL version now extend to the TNT version. However, in this case, the difficulties are due to negative turbulence quantities appearing in course of the iterative solution procedure. Therefore, we did not include the MS2B in the complete flow field calculations performed for the TNT and BSL versions of the k–ω model. In the calculations performed with the manufactured v_t, we have dropped the B from the designation, because the specified v_t fields of MS4 and MS2 are equal to those of MS4B and MS2B.

The grid convergence of the RMS error of u_x is presented in Figure 16 for the two versions of the k–ω model and the four MSs. The TNT and BSL versions of the k–ω exhibit the same trends for the convergence of u_x, which is clearly less dependent on the selected MS than for the Spalart & Allmaras one-equation model. The main features exhibited by the data are:

- All the cases present a well-established observed order of accuracy equal to the theoretical order of the method, that is $p = 2$.
- The constant that defines the error level, α in Equation (21), is clearly dependent on the selected MS.

— The largest α (largest errors) is obtained for the MS4B. This is somehow surprising, because in MS4 and MS2 ω goes to infinity at the wall. This confirms the trend observed in the previous exercise (calculation of the k and ω transport equations using the manufactured velocity field), indicating that the problems caused by the boundary condition of ω are confined to a small vicinity of the bottom.

— The MS4, MS2 and MS1B exhibit smaller values of α for the complete flow field calculations than in the calculations using the manufactured eddy viscosity.

DOI: 10.1002/fld

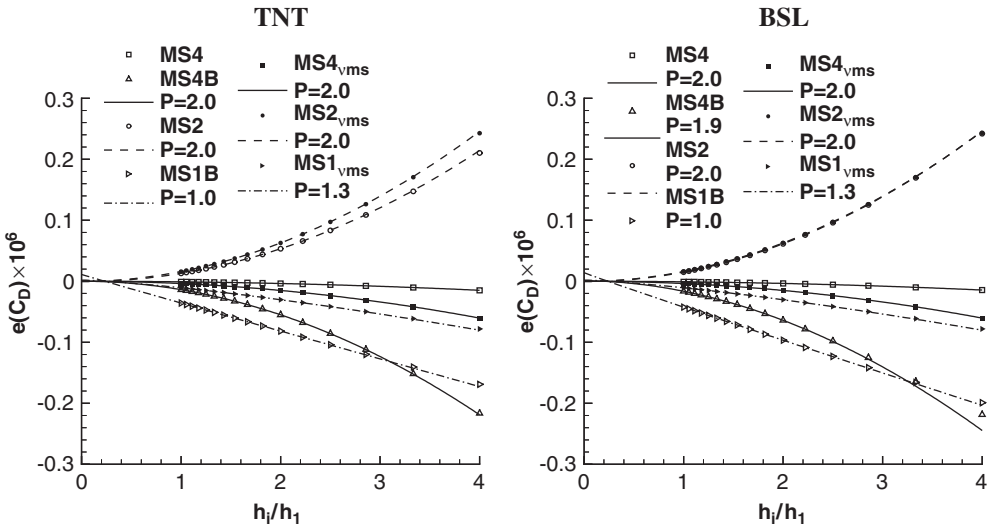

Figure 17. Grid convergence of the error of the friction resistance coefficient at the wall, C_D. TNT and BSL k–ω models.

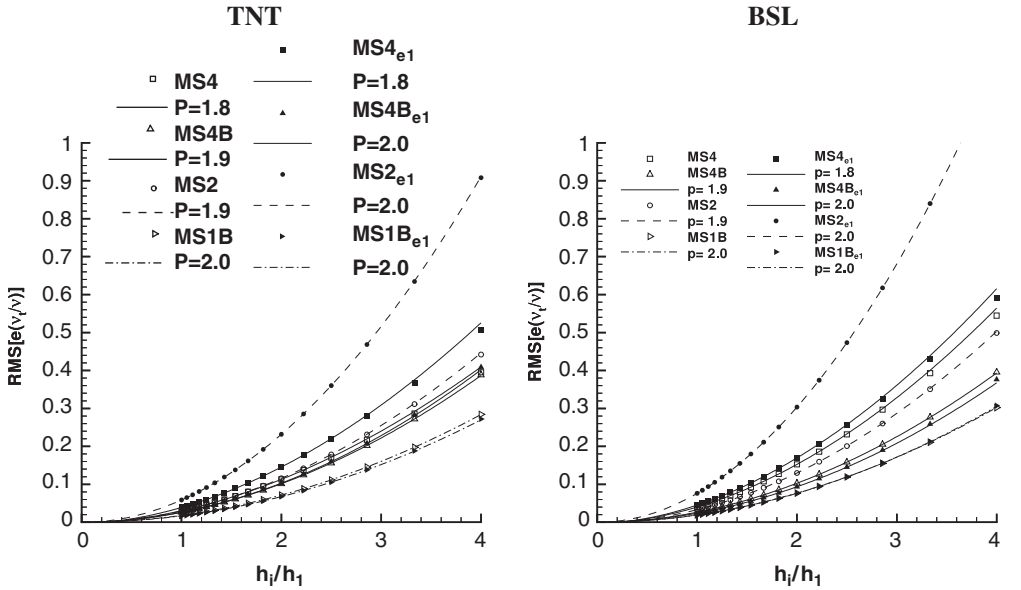

Figure 18. Grid convergence of the RMS error of the eddy-viscosity, v_t. TNT and BSL k–ω models.

Figure 17 presents the error of the 'friction' resistance coefficient at the wall, C_D, as a function of the grid refinement. As for the RMS error of u_x, the two versions of the k–ω model exhibit the

DOI: 10.1002/fld

same trends. However, these are not the same as observed for u_x.

- The MS4, MS4B and MS2 exhibit the expected observed order of accuracy of 2.0. On the other hand, the MS1B leads to first-order p and an inconsistent extrapolation to zero grid size, which is a consequence of the dependence of p on the group of grids selected for its determination.
- This awkward result for MS1B was already present in the calculations performed with the manufactured eddy-viscosity field, where the value of p was only of 1.3. This is really a surprising result because the velocity field is the same for the three MSs and the lowest error level is obtained for the highest-order definition of v_t, MS4.
- Only MS4 presents an error level of the complete flow field calculation below the corresponding calculation with the manufactured v_t. This is a remarkable result, because the most difficult near-wall variation of ω is exactly the one of MS4.

The convergence of the RMS errors of v_t of the calculations with and without calculating the velocity field is compared in Figure 18. The trends observed in the two types of exercises are qualitatively equivalent. However, it is curious that the range of the error level for the four MSs is larger for the solutions using the manufactured velocity field than for the complete flow field calculations. Furthermore, the comparison of error level of the four MSs is not identical for v_t and u_x. The only systematic trend is that the MS1B leads to the smallest level of the error.

4. CONCLUSIONS

This paper presents MSs for the one-equation model of Spalart & Allmaras and the TNT and BSL versions of the two-equation k–ω eddy-viscosity models. The two velocity components and the pressure are identical for all the MSs but various alternatives were tested for the eddy-viscosity and turbulence quantities pertinent to the turbulence models.

For the Spalart & Allmaras one-equation model, we have tested three different fields of the dependent variable, $\tilde{\nu}$. They differ in the near-wall behaviour of $\tilde{\nu}$, which can vary as $\sim y^4$, y^2 or y^1 where y is the distance to the wall.

The three $\tilde{\nu}$ manufactured fields for the Spalart & Allmaras model were also used as eddy-viscosity fields, v_t, for the TNT and BSL versions of the k–ω model. The manufactured turbulence kinetic energy, k, was defined in two ways: an equation similar to the eddy-viscosity but with a lower order dependency on the distance to the wall; or Bradshaw's hypothesis for turbulence in equilibrium defining k as a function of the eddy-viscosity and the strain rate. The second variable ω is calculated from the specified v_t and k: $\omega = k/v_t$. With the two options tested for k, we have fields of ω that are singular at the wall (with variation in y^{-2}, y^{-1}) and non-singular fields with finite values of ω at the wall.

In this paper, we have presented results of three types of calculations: solution of the turbulence quantities transport equations using the manufactured velocity field; solution of the continuity and momentum equations using the manufactured eddy-viscosity field; solution of the complete flow field. The results, obtained with a second-order accurate method, show that the construction of MSs for turbulence models is a delicate matter.

We have observed an unexpectedly high sensitivity of the Spalart & Allmaras model to the manufactured field of the dependent variable, $\tilde{\nu}$. The original MS proposed in [8] leads to convergence difficulties near the wall, which are linked to $\tilde{\nu}$ behaving as y^4 near the wall in the MS4. The

DOI: 10.1002/fld

poor convergence properties obtained for the eddy-viscosity are reflected in the convergence of the velocity and pressure field. An alternative MS with a y^2 dependence in the 'near-wall' region significantly improves the convergence properties of the Spalart & Allmaras model. Finally, an MS with a linear variation with the distance to the wall leads to severe numerical problems, which were traced to the dissipation term.

The convergence properties obtained for the two versions of the k–ω model are much less sensitive to the choice of MS than those of the one-equation model of Spalart & Allmaras. However, some numerical difficulties were encountered. In particular, it is difficult to reproduce the expected behaviour of the blending function of the BSL model, which sometimes causes kinks or oscillations in the manufactured cross-diffusion term.

Specifying k from Bradshaw's equilibrium hypothesis is an elegant way to define k, but it does not lead to the behaviour of ω representative of a near-wall turbulent flow. With the correct ω boundary condition at the wall ($\omega = \infty$) there are locally significant errors in the ω solution. However, in the present MS, this does not affect the calculation of the other flow quantities, including the friction resistance coefficient at the wall.

The grid dependency studies performed for the MSs have also indicated some difficulties for error estimation procedures:

- The convergence properties (error level and observed order of accuracy) may be strongly dependent on the behaviour of the dependent variable of the turbulence model. Furthermore, the observed order of accuracy of the turbulence quantities may be significantly different from the theoretical order of the numerical method adopted.
- The observed order of accuracy of the turbulence quantities may not be uniform over the whole flow field. This means that the observed order of accuracy of the RMS may not be representative of the local convergence properties.
- The convergence properties of the eddy-viscosity may be affected by the damping functions of the turbulence models.

APPENDIX A. SOURCE TERMS OF THE TURBULENCE QUANTITIES TRANSPORT EQUATIONS

A.1. Spalart & Allmaras one-equation model

The Spalart & Allmaras model proposed in [9] solves the following transport equation:

$$u_x \frac{\partial \tilde{\nu}}{\partial x} + u_y \frac{\partial \tilde{\nu}}{\partial y} = c_{b1} \tilde{S} \tilde{\nu} + \frac{1}{\sigma_s} [\nabla \cdot ((\nu + \tilde{\nu}) \nabla \tilde{\nu}) + c_{b2} (\nabla \tilde{\nu} \cdot \nabla \tilde{\nu})] - c_{w1} f_w \left[\frac{\tilde{\nu}}{d} \right]^2 \tag{A1}$$

where

$$S_\Omega = \left| \frac{\partial u_x}{\partial y} - \frac{\partial u_y}{\partial x} \right|$$

$$\tilde{S} = S_\Omega + \frac{\tilde{\nu}}{\kappa^2 d^2} f_{v2}$$

$$d = y$$

DOI: 10.1002/fld

$$f_w = g\left[\frac{1+c_{w3}^6}{g^6+c_{w3}^6}\right]^{1/6}$$

$$f_{v2} = 1 - \frac{\chi}{1+\chi f_{v1}}$$

$$g = r + c_{w2}(r^6 - r)$$

$$r = \frac{\tilde{\nu}}{\tilde{S}\kappa^2 d^2}$$

$$\chi = \frac{\tilde{\nu}}{\nu}$$

$$f_{v1} = \frac{\chi^3}{\chi^3 + c_{v1}^3} \tag{A2}$$

The eddy-viscosity is obtained from

$$\nu_t = \tilde{\nu} f_{v1} \tag{A3}$$

The model constants are:

$$\kappa = 0.41, \quad c_{b1} = 0.1355, \quad c_{b2} = 0.622$$

$$c_{w1} = 3.2391, \quad c_{w2} = 0.3, \quad c_{w3} = 2$$

$$c_{v1} = 7.1, \quad \sigma_s = \tfrac{2}{3}$$

The source function to be added to the right-hand side of the transport equation of $\tilde{\nu}$, Equation (A1), is given by

$$f_{\text{spal}} = T_{\text{cs}} + T_{\text{ds}} + T_{\text{ps}} + T_{\text{dis}} \tag{A4}$$

where

$$\begin{aligned}
T_{\text{cs}} &= u\frac{\partial \tilde{\nu}}{\partial x} + v\frac{\partial \tilde{\nu}}{\partial y} \\
T_{\text{ds}} &= -\frac{1}{\sigma_s}\left[(\nu+\tilde{\nu})\left(\frac{\partial^2 \tilde{\nu}}{\partial x^2} + \frac{\partial^2 \tilde{\nu}}{\partial y^2}\right) + (1+c_{b2})\left(\left(\frac{\partial \tilde{\nu}}{\partial x}\right)^2 + \left(\frac{\partial \tilde{\nu}}{\partial y}\right)^2\right)\right] \\
T_{\text{ps}} &= -c_{b1}\tilde{S}\tilde{\nu} \\
T_{\text{dis}} &= c_{w1} f_w \left[\frac{\tilde{\nu}}{d}\right]^2
\end{aligned} \tag{A5}$$

DOI: 10.1002/fld

The first and second derivatives of $\tilde{\nu}$ with respect to x and y are given by

- MS4 definition of $\tilde{\nu}$, Equation (9)
  - — First derivatives

$$\frac{\partial\tilde{\nu}}{\partial x} = 2\frac{\tilde{\nu}}{x}(\eta_v^2 - 2)$$
$$\frac{\partial\tilde{\nu}}{\partial y} = 2\frac{\tilde{\nu}}{y}(2 - \eta_v^2) \tag{A6}$$

  - — Second derivatives

$$\frac{\partial^2\tilde{\nu}}{\partial x^2} = 2\frac{\tilde{\nu}}{x^2}(2\eta_v^4 - 11\eta_v^2 + 10)$$
$$\frac{\partial^2\tilde{\nu}}{\partial y^2} = 2\frac{\tilde{\nu}}{y^2}(2\eta_v^4 - 9\eta_v^2 + 6) \tag{A7}$$

- MS2 definition of $\tilde{\nu}$, Equation (11)
  - — First derivatives

$$\frac{\partial\tilde{\nu}}{\partial x} = 2\frac{\tilde{\nu}}{x}(\eta_v^2 - 1)$$
$$\frac{\partial\tilde{\nu}}{\partial y} = 2\frac{\tilde{\nu}}{y}(1 - \eta_v^2) \tag{A8}$$

  - — Second derivatives

$$\frac{\partial^2\tilde{\nu}}{\partial x^2} = 2\frac{\tilde{\nu}}{x^2}(2\eta_v^4 - 7\eta_v^2 + 3)$$
$$\frac{\partial^2\tilde{\nu}}{\partial y^2} = 2\frac{\tilde{\nu}}{y^2}(2\eta_v^4 - 5\eta_v^2 + 1) \tag{A9}$$

- MS1 definition of $\tilde{\nu}$, Equation (12)
  - — First derivatives

$$\frac{\partial\tilde{\nu}}{\partial x} = \frac{\tilde{\nu}}{x}(2\eta_v^2 - 1)$$
$$\frac{\partial\tilde{\nu}}{\partial y} = \frac{\tilde{\nu}}{y}(1 - 2\eta_v^2) \tag{A10}$$

  - — Second derivatives

$$\frac{\partial^2\tilde{\nu}}{\partial x^2} = 2\frac{\tilde{\nu}}{x^2}(2\eta_v^4 - 5\eta_v^2 + 1)$$
$$\frac{\partial^2\tilde{\nu}}{\partial y^2} = 2\frac{\tilde{\nu}}{y^2}(2\eta_v^4 - 3\eta_v^2) \tag{A11}$$

DOI: 10.1002/fld

A.1.1. Maximum and minimum values of the different terms of the transport equations

	Convection		Diffusion		Pressure		Source term	
	Min	Max	Min	Max	Min	Max	Min	Max
x momentum equation								
MS4	−0.41	0.000	−0.21	0.16	0.000	0.11	−0.28	0.11
MS2	−0.41	0.000	−0.27	0.18	0.000	0.11	−0.30	0.11
MS1	−0.41	0.000	−0.44	0.19	0.000	0.11	−0.33	0.11

	Convection		Diffusion		Pressure		Source Term	
	Min	Max	Min	Max	Min	Max	Min	Max
y momentum equation								
MS4	−0.11	0.00	−0.03	0.02	−0.07	0.00	−0.13	0.00
MS2	−0.11	0.00	−0.03	0.02	−0.07	0.00	−0.13	0.00
MS1	−0.11	0.00	−0.02	0.02	−0.07	0.00	−0.13	0.00

	$T_{cs} \times 10^3$		$T_{ds} \times 10^3$		$T_{ps} \times 10^3$		$T_{dis} \times 10^3$		$f_{spal} \times 10^3$	
	Min	Max	Min	Max	Min	Max	Min	Max	Min	Max
$\tilde{\nu}$ transport equation										
MS4	−0.62	1.79	−2.15	2.46	−0.92	0.00	0.00	0.11	−3.07	1.66
MS2	−0.26	1.18	−2.62	2.46	−1.06	0.00	0.00	0.63	−2.69	1.66
MS1	−0.10	0.82	−5.28	2.50	−1.14	0.04	0.00	14.09	−0.97	9.44

A.2. TNT and BSL k–ω two-equation models

The TNT, [13], and BSL, [14], k–ω models solve the following transport equations:

$$u\frac{\partial k}{\partial x} + v\frac{\partial k}{\partial y} = v_t S + \nabla \cdot \left(\left(\nu + \frac{\nu_t}{\sigma_k} \right) \nabla k \right) - \beta^* \omega k \tag{A12}$$

$$u\frac{\partial \omega}{\partial x} + v\frac{\partial \omega}{\partial y} = \alpha S + \nabla \cdot \left(\left(\nu + \frac{\nu_t}{\sigma_\omega} \right) \nabla \omega \right) - \beta \omega^2 + F_\omega \frac{1}{\omega} \nabla k \cdot \nabla \omega \tag{A13}$$

For the TNT version, the model constants are

$$\beta^* = 0.09, \quad \beta = 0.075, \quad \alpha = \frac{\beta}{\beta^*} - \frac{\kappa^2}{\sigma_\omega \sqrt{\beta^*}}$$

$$\sigma_k = 1.5, \quad \sigma_\omega = 2, \quad \kappa = 0.41$$

DOI: 10.1002/fld

$$F_\omega = 0.5 \quad \text{if } \nabla k \cdot \nabla \omega > 0$$
$$F_\omega = 0 \quad \text{if } \nabla k \cdot \nabla \omega < 0$$

In the BSL case, we have

$$\alpha = F_1\alpha_1 + (1 - F_1)\alpha_2, \quad \alpha = F_1\beta_1 + (1 - F_1)\beta_2$$
$$\sigma_k = F_1\sigma_{k1} + (1 - F_1)\sigma_{k2}, \quad \sigma_\omega = F_1\sigma_{\omega 1} + (1 - F_1)\sigma_{\omega 2}$$
$$\beta^* = 0.09, \quad \kappa = 0.41$$
$$F_\omega = \frac{2(1 - F_1)}{\sigma_{\omega 2}}$$
$$\alpha_1 = \frac{\beta_1}{\beta^*} - \frac{\kappa^2}{\sigma_{\omega 1}\sqrt{\beta^*}}, \quad \alpha_2 = \frac{\beta_2}{\beta^*} - \frac{\kappa^2}{\sigma_{\omega 2}\sqrt{\beta^*}}$$
$$\beta_1 = 0.075, \quad \beta_2 = 0.0828$$
$$\sigma_{k1} = 2, \quad \sigma_{k2} = 1$$
$$\sigma_{\omega 1} = 2, \quad \sigma_{\omega 2} = \frac{1}{0.856}$$

The blending function F_1 is given by

$$F_1 = \tanh(\arg_1^4) \tag{A14}$$

where

$$\arg_1 = \min\left[\max\left(\frac{\sqrt{k}}{0.09\omega y}, \frac{500\nu}{\omega y^2}\right), \frac{4k}{\sigma_{\omega 2} CD_{k\omega} y^2}\right] \tag{A15}$$

and

$$CD_{k\omega} = \max\left(\frac{2}{\sigma_{\omega 2}\omega}\nabla k \cdot \nabla \omega, 10^{-20}\right) \tag{A16}$$

The satisfaction of the manufactured solutions requires source terms to be added to the k and ω transport equations, which in this case are:

$$f_{k\omega t} = T_{ck\omega t} + T_{dk\omega t} + T_{pk\omega t} + T_{dik\omega t}$$
$$f_{\omega t} = T_{c\omega t} + T_{d\omega t} + T_{p\omega t} + T_{di\omega t} \tag{A17}$$

$$T_{ck\omega t} = u\frac{\partial k}{\partial x} + v\frac{\partial k}{\partial y}$$
$$T_{dk\omega t} = -\left[\left(\nu + \frac{\nu_t}{\sigma_k}\right)\left(\frac{\partial^2 k}{\partial x^2} + \frac{\partial^2 k}{\partial y^2}\right) + \frac{1}{\sigma_k}\left(\frac{\partial \nu_t}{\partial x}\frac{\partial k}{\partial x} + \frac{\partial \nu_t}{\partial y}\frac{\partial k}{\partial y}\right)\right] \tag{A18}$$
$$T_{pk\omega t} = -\nu_t S$$
$$T_{dik\omega t} = \beta^* \omega k$$

DOI: 10.1002/fld

$$
\begin{aligned}
T_{c\omega t} &= u\frac{\partial \omega}{\partial x} + v\frac{\partial \omega}{\partial y} \\
T_{d\omega t} &= -\left[\left(\nu + \frac{\nu_t}{\sigma_\omega}\right)\left(\frac{\partial^2 \omega}{\partial x^2} + \frac{\partial^2 \omega}{\partial y^2}\right) + \frac{1}{\sigma_\omega}\left(\frac{\partial \nu_t}{\partial x}\frac{\partial \omega}{\partial x} + \frac{\partial \nu_t}{\partial y}\frac{\partial \omega}{\partial y}\right)\right] \\
T_{p\omega t} &= -\alpha S \\
T_{di\omega t} &= \beta\omega^2 - F_\omega \frac{1}{\omega}\nabla k \cdot \nabla \omega
\end{aligned}
\tag{A19}
$$

In order to avoid problems due to the discontinuities of the derivatives of the blending function F_1, we have taken $\sigma_k = \sigma_{k1}$ and $\sigma_\omega = \sigma_{\omega 1}$ in the BSL version.

The derivatives of ν_t are equivalent to the ones given above for $\tilde{\nu}$. The first and second derivatives of k and ω for the five MSs are listed below.

- MS4
  - — k defined by Equation (17):
    - ∗ First derivatives

$$
\begin{aligned}
\frac{\partial k}{\partial x} &= 2\frac{k}{x}\left(\eta_\nu^2 - 1\right) \\
\frac{\partial k}{\partial y} &= 2\frac{k}{y}(1 - \eta_\nu^2)
\end{aligned}
\tag{A20}
$$

    - ∗ Second derivatives

$$
\begin{aligned}
\frac{\partial^2 k}{\partial x^2} &= 2\frac{k}{x^2}(2\eta_\nu^4 - 7\eta_\nu^2 + 3) \\
\frac{\partial^2 k}{\partial y^2} &= 2\frac{k}{y^2}(2\eta_\nu^4 - 5\eta_\nu^2 + 1)
\end{aligned}
\tag{A21}
$$

  - — ω defined by Equation (18):
    - ∗ First derivatives

$$
\begin{aligned}
\frac{\partial \omega}{\partial x} &= \frac{2\omega}{x} \\
\frac{\partial \omega}{\partial y} &= -\frac{2\omega}{y}
\end{aligned}
\tag{A22}
$$

    - ∗ Second derivatives

$$
\begin{aligned}
\frac{\partial^2 \omega}{\partial x^2} &= \frac{2\omega}{x^2} \\
\frac{\partial^2 \omega}{\partial y^2} &= \frac{6\omega}{y^2}
\end{aligned}
\tag{A23}
$$

DOI: 10.1002/fld

- MS2
  - — k defined by Equation (19):
    - * First derivatives

$$\frac{\partial k}{\partial x} = \frac{k}{x}(2\eta_v^2 - 1)$$
$$\frac{\partial k}{\partial y} = \frac{k}{y}(1 - 2\eta_v^2) \tag{A24}$$

    - * Second derivatives

$$\frac{\partial^2 k}{\partial x^2} = 2\frac{k}{x^2}(2\eta_v^4 - 5\eta_v^2 + 1)$$
$$\frac{\partial^2 k}{\partial y^2} = 2\frac{k}{y^2}(2\eta_v^4 - 3\eta_v^2) \tag{A25}$$

  - — ω defined by Equation (20):
    - * First derivatives

$$\frac{\partial \omega}{\partial x} = \frac{\omega}{x}$$
$$\frac{\partial \omega}{\partial y} = -\frac{\omega}{y} \tag{A26}$$

    - * Second derivatives

$$\frac{\partial^2 \omega}{\partial x^2} = 0$$
$$\frac{\partial^2 \omega}{\partial y^2} = \frac{2\omega}{y^2} \tag{A27}$$

- MS4B, MS2B and MS1B
  - — k defined by Equation (13):
    - * First derivatives

$$\frac{\partial k}{\partial x} = \frac{1}{0.3}\left(v_t \frac{\partial S}{\partial x} + S\frac{\partial v_t}{\partial x}\right)$$
$$\frac{\partial k}{\partial y} = \frac{1}{0.3}\left(v_t \frac{\partial S}{\partial y} + S\frac{\partial v_t}{\partial y}\right) \tag{A28}$$

    - * Second derivatives

$$\frac{\partial^2 k}{\partial x^2} = \frac{1}{0.3}\left(v_t \frac{\partial^2 S}{\partial x^2} + 2\frac{\partial S}{\partial x}\frac{\partial v_t}{\partial x} + S\frac{\partial^2 v_t}{\partial x^2}\right)$$
$$\frac{\partial^2 k}{\partial y^2} = \frac{1}{0.3}\left(v_t \frac{\partial^2 S}{\partial y^2} + 2\frac{\partial S}{\partial y}\frac{\partial v_t}{\partial y} + S\frac{\partial^2 v_t}{\partial y^2}\right) \tag{A29}$$

DOI: 10.1002/fld

— ω defined by Equation (16):
  * First derivatives

$$\frac{\partial \omega}{\partial x} = \frac{1}{0.3}\frac{\partial S}{\partial x}$$
$$\frac{\partial k}{\partial y} = \frac{1}{0.3}\frac{\partial S}{\partial y} \tag{A30}$$

  * Second derivatives

$$\frac{\partial^2 \omega}{\partial x^2} = \frac{1}{0.3}\frac{\partial^2 S}{\partial x^2}$$
$$\frac{\partial^2 \omega}{\partial y^2} = \frac{1}{0.3}\frac{\partial^2 S}{\partial y^2} \tag{A31}$$

— Strain rate, S, Equation (14).
  * First derivatives

$$\frac{\partial S}{\partial x} = \frac{\partial^2 u_x}{\partial x \partial y} + \frac{\partial^2 u_y}{\partial x^2}$$
$$\frac{\partial S}{\partial y} = \frac{\partial^2 u_x}{\partial y^2} + \frac{\partial^2 u_y}{\partial x \partial y} \tag{A32}$$

  * Second derivatives

$$\frac{\partial^2 S}{\partial x^2} = \frac{\partial^3 u_x}{\partial x^2 \partial y} + \frac{\partial^3 u_y}{\partial x^3}$$
$$\frac{\partial^2 S}{\partial y^2} = \frac{\partial^3 u_x}{\partial y^3} + \frac{\partial^3 u_y}{\partial x \partial y^2} \tag{A33}$$

A.2.1. Maximum and minimum values of the different terms of the transport equations

TNT	Convection		Diffusion		Pressure		Source term	
BSL	Min	Max	Min	Max	Min	Max	Min	Max
x momentum equation								
MS4, MS4B	−0.41	0.00	−0.21	0.16	0.00	0.11	−0.28	0.11
MS2, MS2B	−0.41	0.00	−0.27	0.18	0.00	0.11	−0.30	0.10
MS1B	−0.41	0.00	−0.42	0.19	0.00	0.11	−0.31	0.11

DOI: 10.1002/fld

TNT	Convection		Diffusion		Pressure		Source term	
BSL	Min	Max	Min	Max	Min	Max	Min	Max
y momentum equation								
MS4, MS4B	−0.11	0.00	−0.03	0.02	−0.07	0.00	−0.13	0.00
MS2, MS2B	−0.11	0.00	−0.03	0.02	−0.07	0.00	−0.13	0.00
MS1B	−0.11	0.00	−0.02	0.02	−0.07	0.00	−0.13	0.00

TNT	$T_{ck\omega t} \times 10^3$		$T_{dk\omega t} \times 10^3$		$T_{pk\omega t} \times 10^3$		$T_{dik\omega t} \times 10^3$		$f_{k\omega t} \times 10^3$	
	Min	Max	Min	Max	Min	Max	Min	Max	Min	Max
k transport equation										
MS4	−2.59	11.77	−4.99	8.71	−48.11	0.00	0.00	36.00	−28.97	35.99
MS2	−1.03	8.24	−4.84	9.21	−62.55	0.00	0.00	18.00	−45.26	17.96
MS4B	−29.53	24.09	−14.05	27.09	−48.11	0.00	0.00	45.28	−33.26	13.97
MS2B	−21.73	16.83	−20.57	31.90	−62.55	0.00	0.00	60.68	−27.63	9.43
MS1B	−16.02	11.82	−43.43	35.31	−71.33	0.00	0.00	70.25	−43.44	18.48
BSL	$T_{ck\omega t} \times 10^3$		$T_{dk\omega t} \times 10^3$		$T_{pk\omega t} \times 10^3$		$T_{dik\omega t} \times 10^3$		$f_{k\omega t} \times 10^3$	
	Min	Max	Min	Max	Min	Max	Min	Max	Min	Max
MS4	−2.59	11.77	−3.74	6.54	−48.11	0.00	0.00	36.00	−30.13	35.99
MS2	−1.03	8.24	−3.63	6.91	−62.55	0.00	0.00	18.00	−46.74	17.97
MS4B	−29.53	24.09	−10.54	20.33	−48.11	0.00	0.00	45.28	−30.77	15.68
MS2B	−21.73	16.83	−15.43	23.93	−62.55	0.00	0.00	60.68	−22.93	10.50
MS1B	−16.02	11.82	−32.57	26.50	−71.33	0.00	0.00	70.25	−32.58	9.71

TNT	$T_{c\omega t}$		$T_{d\omega t}$		$T_{p\omega t}$		$T_{di\omega t}$		$f_{k\omega t}$	
	Min	Max	Min	Max	Min	Max	Min	Max	Min	Max
ω transport equation										
MS4	0.51	>100	$\to\infty$	5.03	−44.98	0.00	−0.43	$\to\infty$	−19.37	$\to\infty$
MS2	1.23	3.87	$\to\infty$	0.00	−44.98	0.00	0.06	$\to\infty$	−29.87	$\to\infty$
MS4B	−17.98	11.84	−2.46	3.06	−44.98	0.00	0.00	67.77	−9.83	22.52
MS2B	−17.98	11.84	−2.08	2.78	−44.98	0.00	0.00	67.77	−10.98	22.52
MS1B	−17.98	11.84	−1.70	2.48	−44.98	0.00	0.00	67.77	−10.26	22.61
BSL	$T_{c\omega t}$		$T_{d\omega t}$		$T_{p\omega t}$		$T_{di\omega t}$		$f_{k\omega t}$	
	Min	Max	Min	Max	Min	Max	Min	Max	Min	Max
MS4	0.51	>100	$\to\infty$	5.03	−36.85	0.00	−6.42	$\to\infty$	−20.68	$\to\infty$
MS2	1.23	3.87	$\to\infty$	0.00	−44.98	0.00	−0.94	$\to\infty$	−28.66	$\to\infty$
MS4B	−17.98	11.84	−2.46	3.06	−44.98	0.00	0.00	74.25	−11.42	34.89
MS2B	−17.98	11.84	−2.08	2.78	−44.98	0.00	0.00	67.77	−9.99	22.52
MS1B	−17.98	11.84	−1.70	2.48	−44.98	0.00	0.00	67.77	−7.51	22.61

DOI: 10.1002/fld

REFERENCES

1. Pelletier D, Roache PJ. CFD code verification and the method of the manufactured solutions. *10th Annual Conference of the CFD Society of Canada*, Windsor, Ont., Canada, June 2002.
2. Oberkampf WL, Blottner FG, Aeschliman DP. Methodology for computational fluid dynamics code verification/validation. *AIAA 26th Fluid Dynamics Conference*, *AIAA Paper 95-2226*, San Diego, CA, June 1995.
3. Roache PJ. *Verification and Validation in Computational Science and Engineering*. Hermosa Publishers: Albuquerque, NM, U.S.A., 1998.
4. Turgeon É, Pelletier D. Verification and validation of adaptive finite element method for impingement heat transfer. *Journal of Thermophysics and Heat Transfer* 2001; **15**:284–292.
5. Turgeon É, Pelletier D. Verification and validation in CFD using an adaptive finite element method. *Canadian Aeronautic and Space Journal* 2002; **48**:219–231.
6. Knupp P, Salari K. *Verification of Computer Codes in Computational Science and Engineering*. CRC Press: Boca Raton, FL, 2002.
7. Roache PJ. Code verification by the method of the manufactured solutions. *Journal of Fluids Engineering* (ASME) 2002; **114**:4–10.
8. Eça L, Hoekstra M, Hay A, Pelletier D. A manufactured solution for a two-dimensional steady wall-bounded incompressible turbulent flow. *IST Report D72-34*, *EPM Report EMP-RT-2005-08*, November 2005.
9. Spalart PR, Allmaras SR. A one-equations turbulence model for aerodynamic flows. *AIAA 30th Aerospace Sciences Meeting*, Reno, January 1992.
10. Menter FR. Eddy-viscosity transport equations and their relation to the k–ε model. *Journal of Fluids Engineering* 1997; **119**:876–884.
11. Launder BE, Spalding DB. The numerical computation of turbulent flows. *Computer Methods in Applied Mechanics and Engineering* 1974; **3**:269–289.
12. Chien KY. Prediction of channel and boundary-layer flows with a low-Reynolds-number turbulence model. *AIAA Journal* 1982; **20**:33–38.
13. Kok JC. Resolving the dependence on free-stream values for the k–ω turbulence model. NLR-TP-99295, 1999.
14. Menter FR. Two-equation eddy-viscosity turbulence models for engineering applications. *AIAA Journal* 1994; **32**:1598–1605.
15. José MQB Jacob, Eça L. 2-D incompressible steady flow calculations with a fully coupled method. *VI Congresso Nacional de Mecânica Aplicada e Computacional*, Aveiro, April 2000.
16. Eça L. Calculation of a manufactured solution for a 2-D steady incompressible near-wall turbulent flow with PARNASSOS. *IST Report D72-35*, January 2006.
17. Saad Y, Schultz MH. GMRES: a generalized minimum residual algorithm for solving nonsymmetric linear systems. *SIAM Journal on Science and Statistical Computation* 1986; **7**:856–869.
18. Eça L, Hoekstra M, Hay A, Pelletier D. Manufactured solutions for one-equation turbulence models in a two-dimensional steady wall-bounded incompressible turbulent flow. *IST Report D72-36*, *EPM Report EMP-RT-2006-02*, February 2006.
19. Vinokur M. On one-dimensional stretching functions for finite-difference calculations. *Journal of Computational Physics* 1983; **50**:215–234.
20. Eça L, Hoekstra M. An evaluation of verification procedures for CFD applications. *24th Symposium on Naval Hydrodynamics*, Fukuoka, Japan, July 2002.
21. Wilcox DC. *Turbulence Modeling for CFD* (2nd edn). DCW Industries: March 2000.
22. Eça L, Hoekstra M. On the influence of the iterative error in the numerical uncertainty of ship viscous flow calculations. *26th Symposium on Naval Hydrodynamics*, Rome, Italy, September 2006.
23. Eça L, Hoekstra M. On the grid sensitivity of the wall boundary condition of the k–ω model. *Journal of Fluids Engineering* 2004; **126**(6):900–910.

DOI: 10.1002/fld